The magnetic anisotropy and spin reorientation of nanostructures and nanoscale films

2004 J. Phys.: Condens. Matter 16 R603

(http://iopscience.iop.org/0953-8984/16/20/R01)

INSTITUTE OF PHYSICS PUBLISHING JOURNAL OF PHYSICS: CONDENSED MATTER

J. Phys.: Condens. Matter **16** (2004) R603–R636 PII: S0953-8984(04)35569-4

TOPICAL REVIEW

The magnetic anisotropy and spin reorientation of nanostructures and nanoscale films

D Sander

Max-Planck-Institut für Mikrostrukturphysik, Weinberg 2, D-06120 Halle, Germany

E-mail: sander@mpi-halle.de

Received 2 December 2003
Published 7 May 2004
Online at stacks.iop.org/JPhysCM/16/R603
DOI: 10.1088/0953-8984/16/20/R01

Abstract

The magnetic anisotropy of nanometer thin films and of nanosize structures is discussed. Experimental methods for the quantitative determination of magnetic anisotropy are described. Magnetocrystalline, shape, and magnetoelastic anisotropy contributions are reviewed, and recent examples for the non-bulk-like magnetic anisotropy and of the temperature dependence of both the magnetization and magnetic anisotropy of nanoscale materials are presented. It is shown that film strain and its relaxation give rise to film thickness dependent anisotropy, which can be misinterpreted as a surface anisotropy. The decisive role of the surface anisotropy for adsorbate-induced spin-reorientation transitions (SRT) is elucidated. The application of x-ray magnetic circular dichroism (XMCD) for the determination of magnetic anisotropy of nanosize islands down to the single atom size is presented.

(Some figures in this article are in colour only in the electronic version)

Contents

1. Introduction 604
2. The magnetic anisotropy of bulk and nanoscale samples 604
   2.1. The electronic origin of magnetic anisotropy 605
   2.2. Magnetocrystalline anisotropy 607
   2.3. The magnetic anisotropy of ultrathin films 610
   2.4. Magnetoelastic anisotropy 611
   2.5. Magnetoelastic stress and film stress measurements 611
   2.6. Lattice strain in epitaxial systems 613
   2.7. Film thickness dependent strain 614
   2.8. The magnetoelastic anisotropy of ultrathin films 615
   2.9. Shape anisotropy 617
3. The experimental determination of magnetic anisotropy 622
   3.1. The magnetic circular dichroism of magnetic structures 622

4. The temperature dependence of magnetization and magnetic anisotropy 623
5. The adsorbate-induced spin reorientation transition on ferromagnetic monolayers 625
6. Nano-patterning of magnetic anisotropy 627
6.1. The self-organized tuning of magnetic anisotropy 627
6.2. The magnetic length scale for nanoscale geometrical constrictions 629
7. Magnetic anisotropy on the atomic scale 630
8. Conclusion and outlook 630
Acknowledgments 632
References 632

1. Introduction

The interest in magnetic materials has experienced a tremendous boost due to the versatility of magnetic multilayers for applications in sensors, actuators, and magnetic data storage [1]. Similarly, the recently introduced nonvolatile magnetic random access memory (MRAM) [2, 3], and related MRAM-logic [4], rely on the proper tailoring of the magnetic properties of highly complex multilayer structures.

These examples indicate the high potential of magnetic materials for numerous present and future applications, in addition to the continued interest in traditional fields like transformer steel or permanent magnet applications [5].

No matter what application one is interested in, a key property of a ferromagnetic sample is the direction of its magnetization. In permanent magnets, this direction should be fixed rigidly to ensure proper functioning of the magnet. In sensing applications, such as in read-heads, an easy rotation of the magnetization of a ferromagnetic layer in the faint stray-field of a magnetized hard disk is, however, necessary.

This contribution deals with magnetic anisotropy. This is the quantity which determines the easy magnetization direction of a magnet, and it is also decisive for the magnetization reversal in external fields. In contrast to the sophisticated multilayers described above, the samples, which are discussed in this contribution, are usually epitaxial layers of ferromagnetic materials. The nanosize aspect is considered for ultrathin films, with a thickness of the order of several atomic layers, and for the self-organized formation of nanoscale islands, where the lateral dimensions can be as small as a single atom.

This review is organized as follows. An introduction to the electronic origin of magnetic anisotropy and to the various contributions to the magnetic anisotropy (magnetocrystalline, magnetoelastic, and shape anisotropy) is given in section 2. Special emphasis is devoted to the issue of strain-dependent magnetic anisotropy. Experimental techniques to measure magnetic anisotropy quantitatively are compiled in section 3. Selected examples on the peculiar temperature dependence of the magnetization and magnetic anisotropy of ultrathin films are presented in section 4. In section 5, the influence of an adsorbate coverage on the magnetic anisotropy of ultrathin films is presented. Section 6 describes the nanopatterning of magnetic anisotropy by self-organized growth, and section 7 extends the anisotropy measurement and its discussion to the atomic limit.

2. The magnetic anisotropy of bulk and nanoscale samples

The various contributions to the magnetic anisotropy can be classified according to their physical origin. We distinguish between magnetic anisotropy due to spin–orbit coupling (SOC) as compared to magnetic anisotropy of dipolar origin. The former includes magnetocrystalline

and magnetoelastic anisotropy; the latter is responsible for shape anisotropy. We neglect dipolar crystalline anisotropy due to its small magnitude [6].

Magnetocrystalline anisotropy, magnetoelastic anisotropy, and shape anisotropy have been thoroughly discussed in textbooks on bulk magnetism [7–11], in books on ultrathin film magnetism [6, 12–17], and in several review articles on ferromagnetic layers [18–27], and for magnetic nanostructures [28, 29] and nanowires [30]. Comprehensive data on the magnetic anisotropy of various systems can be found in these references. Critical phenomena are discussed in [23, 28, 31].

In the following, a short overview of the electronic origin of magnetic anisotropy is given. Crystal symmetry, crystal field splitting and spin–orbit interaction are briefly discussed in relation to magnetic anisotropy. The magnetocrystalline anisotropy of bulk samples and of ultrathin films is introduced, and the correlation between lattice strain and magnetic anisotropy is reviewed. Section 2.9 deals with special aspects of the shape anisotropy of anisotropic islands and nanoplatelets.

2.1. The electronic origin of magnetic anisotropy

Magnetocrystalline anisotropy is a direct consequence of spin–orbit coupling. In bulk samples the orbital moment is quenched, and the contribution of the orbital moment to the total magnetic moment is small. This statement is corroborated by measurements of the magnetomechanical ratio g' which has a value of $\approx$1.9 for bulk transition metals, where $g' = 2$ indicates complete quenching of the orbital moment [32, 33]. This means that the magnetism of bulk 3d metals is largely due to the spin moment, and just to a small extent due to the orbital moment. The magnetism in transition metals is ascribed to 3d electrons. Their orbital moment is tightly fixed to the crystal lattice, and it can just orient very little in an external field [34]. The electron spin, however, is weakly coupled to the orbital moment via the spin–orbit coupling, and the energy of the system depends on the relative orientation between the magnetization (spin orientation) and crystal axes.

Experiments on the magnetocrystalline anisotropy of cubic bulk samples reveal that the corresponding energy scales are of the order of a few μeV/atom. This small anisotropy energy makes the calculation of the magnetic anisotropy a demanding task. The calculations require a proper selection of a theoretical model, and demand the highest numerical accuracy. Still, the agreement between calculations and observed anisotropy is not guaranteed, as illustrated by the failure of state-of-the art calculations to reproduce the correct easy magnetization axis of bulk fcc Ni [35, 36].

2.1.1. Magnetic anisotropy and symmetry in perturbation theory. The high symmetry of bulk cubic structures leads to a magnetic anisotropy which is of order four for the lowest order directional dependence of the magnetization. This high symmetry leads to a small magnetic anisotropy as deduced from a perturbative treatment of magnetic anisotropy [6, 18]. In contrast to bulk samples, the magnetic anisotropy of thin (a few atomic layers) ferromagnetic films can be three orders of magnitude larger, and corresponds to an energy of meV/atom.

Perturbation theory suggests that the magnitude of the lowest order anisotropy constant K_1 scales as $K_1 \sim \xi^2/W$ for an uniaxial system, as opposed to $K_1 \sim \xi^4/W^3$ for a cubic system. The spin–orbit constant ξ is of the order of 50–100 meV for 3d metals, and the 3d band width W is of the order of a few eV. These values give the correct order of magnitude of the anisotropy of cubic systems and of ultrathin films. In general, anisotropy constants of order n scale as $(\xi/W)^n$, which is a small quantity, and this explains the increase of magnetic anisotropy for systems of reduced symmetry [6].

The increase of magnetic anisotropy for ultrathin films is often ascribed to so-called interface anisotropy contributions. These interface and surface anisotropy contributions are ascribed to the different atomic environment of atoms near the interface. The symmetry of an interface is generally lower, and this gives rise to anisotropy contributions in lower order of the direction cosines, e.g. order two for cubic (100) surfaces, as compared to order four for cubic bulk structures [6].

Note also that epitaxial strain leads to a reduction of symmetry. A prominent example is the growth of Ni on Cu(001), where the epitaxial misfit leads to a tetragonally distorted Ni film, as discussed below in section 2.6. In general, lattice strain is an important factor which gives rise to an uniaxial anisotropy, as will become clear from the discussion in the following sections. The decisive role of tetragonal distortion for the enhanced magnetic anisotropy has also been confirmed in recent first principles calculations [37].

2.1.2. Magnetic anisotropy, crystal field effects and band filling. The important impact of symmetry on the resulting magnetic anisotropy can also be understood in the crystal field description, which has been applied successfully to describe the magnetic anisotropy of 3d ions [5]. The energetically degenerate 3d levels of a free atom split into two groups, e_g (d_{z^2}, $d_{x^2-y^2}$ orbitals, electron density large along the cubic axes) and t_{2g} (d_{xy}, d_{xz}, d_{yz} orbitals, electron density large between the cubic axes), in the presence of the electric field of the surrounding atoms. The energy separation and the relative positioning of the e_g and t_{2g} levels depend on the symmetry of the atomic arrangement [11], and a tetragonal distortion lifts the degeneracy of these levels [36]. Thus, a change of symmetry, e.g. induced by strain, may lead to a change of the relative occupancy of the different d-orbitals, which in turn leads via spin–orbit coupling to a change of the magnetic anisotropy. The effect of a strain-induced variation of the d-orbital occupancy on the magnetic anisotropy has been corroborated in a first-principles calculation [38], as discussed in section 2.4.

In addition to symmetry, the band filling (number of valence electrons per unit cell) is an important factor which governs the magnetic anisotropy. For example, a band filling which leads to a positioning of the Fermi energy close to the energy of the in-plane oriented orbitals ($d_{x^2-y^2}$, d_{xy}) favours perpendicular magnetization [37, 39]. These predictions of first principles calculations have been experimentally verified for Co–Ni multilayers [39].

2.1.3. Magnetic anisotropy and orbital moment anisotropy. According to perturbation theory, the magnetic anisotropy is correlated with the anisotropy of the orbital moment. This correlation suggests that the easy magnetization direction is the direction of the largest orbital moment [6, 37]. This prediction has been confirmed in first principles calculations of bulk [35] and multilayered systems [37, 40]. X-ray magnetic circular dichroism (XMCD) experiments can be applied to separate spin and orbital moments, and XMCD has been used to investigate the anisotropy of orbital moments [41]. These experimental studies have supported the connection between the orbital moment anisotropy and magnetic anisotropy. Recent experiments show that fully unquenched orbital moments can be obtained for 3d impurities on alkali metal films [42], which is ascribed to the localization of the 3d states of these systems. Record high magnetic anisotropy is observed for samples with large orbital moments [43], and these results are discussed.

2.1.4. A critical remark on magnetic surface anisotropy. The reduced symmetry of surface atoms as compared to bulk atoms gives rise to a magnetic anisotropy different from the respective bulk value. This anisotropy was introduced by Néel, and it is known as Néel-type anisotropy [6]. A surface/interface anisotropy is expected to contribute decisively for

systems which are dominated by their surface properties, e.g. due to very small thickness in the few atomic layers regime. The magnitude of the surface anisotropy is independent of the film thickness. An anisotropy contribution results, which is constant as a function of film thickness, provided that the film thickness variation does not induce a structural or morphological change at the interface layer.

Unfortunately, the important character of a Néel-type surface anisotropy as a constant contribution to the effective anisotropy is disguised by the generally applied separation of the effective anisotropy K_{eff} into so-called volume (K_{V}) and surface (K_{S}) terms. This separation is expressed by writing for the effective anisotropy energy density $K_{\mathrm{eff}} = K_{\mathrm{V}} + 2K_{\mathrm{S}}/t$, where the film thickness is given by t [13, 18, 24].

We raise our concerns about this potentially problematic approach. Although common practice, this separation does not represent the physics behind the surface anisotropy. A true surface/interface anisotropy is a constant contribution to the—probably film-thickness dependent—magnetic anisotropy. A scaling of an anisotropy contribution in proportion to t^{-1} by no means necessarily indicates a true Néel-type surface anisotropy.

It is often assumed [18] that film strain varies in proportion to t^{-1}, and this clear bulk contribution should not be treated as a surface anisotropy. In contrast to the simple strain-decay model, our measurements indicate that a film strain variation in proportion to t^{-1} is not found experimentally. These results question the general applicability of a t^{-1} strain variation for epitaxial films. A further shortcoming of the separation of magnetic anisotropy contributions into volume and surface terms is that in the limit of small film thickness, e.g. one atomic layer, a separation of the sample into bulk and two surfaces does not seem to be appropriate.

It is shown that the apparent thickness dependence of the magnetoelastic anisotropy contribution can be misinterpreted in terms of a surface anisotropy. However, recent measurements of the magnetoelastic coupling identify the modification of the effective magnetoelastic coupling by film strain as the physical origin of this anisotropy variation.

Surface contributions to the magnetic anisotropy as suggested by Néel can be dominant for the resulting magnetic anisotropy. Examples are the hydrogen- and iron-induced reorientation of the easy magnetization direction in Ni monolayers, which indicate the decisive role of an adsorbate coverage for the resulting magnetic anisotropy of ferromagnetic monolayers, and the switching of the easy magnetization direction of Ni(111) from in-plane to out-of-plane by an Fe-coverage is discussed in section 5.

In the following, we concentrate on anisotropy contributions with a special emphasis on nanoscale films and nanopatterns. Here, we present for completeness a compilation of the respective bulk anisotropy data and discuss the corresponding energy scales. We present examples which illustrate how the discussion of magnetic anisotropy in terms of bulk properties has to be extended to describe the magnetic anisotropy on the nanoscale properly.

2.2. Magnetocrystalline anisotropy

The direction of the spontaneous magnetization of crystalline samples is oriented along certain directions. For bulk samples of bcc-Fe, fcc-Ni, and hcp-Co, these are the cubic $\langle 100 \rangle$, $\langle 111 \rangle$ and hexagonal $\langle 0001 \rangle$ directions, respectively. These directions are called easy magnetization directions. Magnetization along another direction requires an excess energy, which can be extracted for example from the effective anisotropy $K_{\mathrm{eff}} = \mu_0 \int H \mathrm{d}M$, as determined from so-called hard-axis magnetization loops [13].

2.2.1. Magnetization along a hard magnetization direction. The orientation of the magnetizing field with respect to the sample can lead to easy-axis or hard-axis magnetization

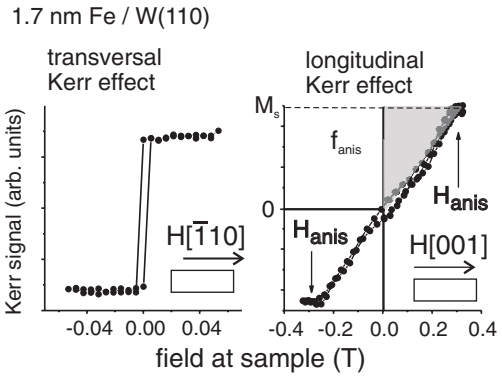

Figure 1. MOKE measurements of a 1.7 nm Fe(110) film, deposited on W(110) [26]. The film was deposited and measured at 300 K. Note that magnetization along the in-plane [$\bar{1}$10] direction leads to a rectangular hysteresis loop, indicative of a easy magnetization direction. Magnetization along the in-plane [001] direction leads to a hard-axis magnetization curve, where the saturation magnetization is reached at the anisotropy field $H_{\rm anis} = 0.3$ T. The in-plane anisotropy energy density $f_{\rm anis}$ is given by the area of the shaded region. Annealing of the film leads to an in-plane SRT to [$\bar{1}$10], as shown in figure 6.

curves. As shown in figure 1, rectangular hysteresis curves with full remanence, or hysteresis-free magnetization curves with zero remanence, are obtained, respectively. The magnetic anisotropy energy density is the excess work which needs to be put into the system to achieve saturation magnetization along a non-easy axis of magnetization. This excess work depends on the orientation of the magnetizing field with respect to the sample, and its magnitude will be different in general for magnetization in-plane, as compared to magnetization out-of-plane. The magnitude of the anisotropy energy density $f_{\rm anis}$ is given by $f_{\rm anis} = \mu_0 \int H \mathrm{d}M$.

Figure 1 shows magnetization curves by MOKE measurements of 1.7 nm Fe, deposited on W(110) at 300 K. The magnetizing field is directed along in-plane [$\bar{1}$10], left-hand panel, and along in-plane [001], right-hand panel. The full remanence at zero field shown in the left-hand panel indicates an easy magnetization direction, whereas the slope of the magnetization curve of the right panel is due to a magnetization along a hard axis.

The value of the in-plane anisotropy given by the integral is given by the shaded area of the right-hand panel in figure 1, and $f_{\rm anis} = 0.5\,\mu_0\,H_{\rm anis}\,M_{\rm s}$. The magnetizing field $\mu_0\,H$ is given in T, the magnetization in A m^{-1}. Our example of figure 1 indicates $\mu_0\,H = 0.3$ T, and with $M_{\rm s} = 1717 \times 10^3$ A m^{-1} from table 7, the in-plane anisotropy follows as $f_{\rm anis} = 0.26$ MJ m^{-3}. This value compares reasonably well with the anisotropy data extracted from TOM measurements [44]. Note that large magnetic fields, beyond typical limits of UHV-operated magnets, might be necessary to drive a sample into saturation magnetization along a hard axis. It will be demonstrated in section 7 that even fields of 7 T, as produced by superconducting magnets, are not necessarily sufficient to achieve such a saturation for a large magnetic anisotropy.

2.2.2. Magnetization in the presence of an additional constant magnetic field. The application of a constant magnetic field along a direction perpendicular to the direction of the magnetizing field was proposed to extract the in-plane anisotropy [45, 46]. This method is demonstrated in the top panel of figure 2. The method can be rationalized by noting that the constant magnetic field at zero magnetizing field creates a uniaxial anisotropy. The magnetization of the sample is oriented along the direction of the constant field. With increasing magnetizing

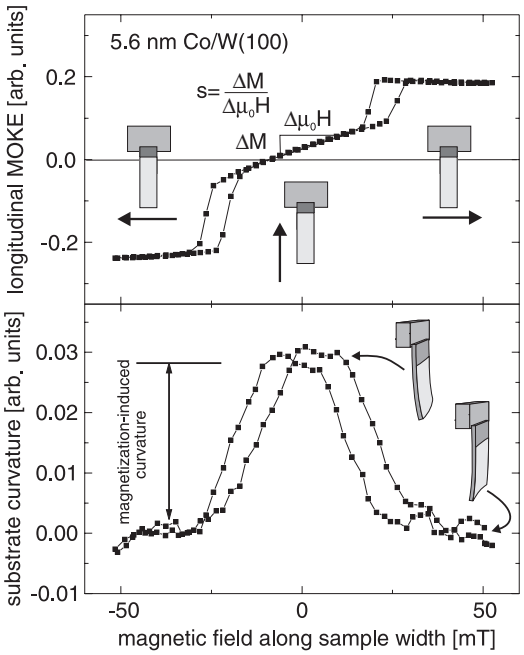

Figure 2. MOKE measurements, top panel, and magnetization-induced curvature, bottom panel, of 5.7 nm Co($11\bar{2}0$) on W(100). The film was deposited and measured at 300 K. The magnetic field is varied along the sample width, and a constant magnetic field of 2 mT is applied along the sample length. From the slope of the MOKE curve around zero horizontal field, s, the fourfold in-plane anisotropy is extracted. The bottom panel shows the simultaneously measured crystal curvature, which is induced by the magnetoelastic stress change upon a magnetization reversal from along the sample length to along the sample width. From this curvature change, the magnetoelastic coupling B_4^{eff} is calculated, as explained in section 2.4.

field along the perpendicular in-plane direction, the magnetization rotates reversibly away from the constant offset-field direction. At the switching field, the magnetization jumps to the fully magnetized state, which is along the direction of the variable magnetizing field. The slope of the magnetization curve around zero magnetizing field, $s = \Delta M/(\Delta\mu_0 H)$ (M is given in units of the saturation magnetization M_s), is used to derive the anisotropy field from $H_{\text{anis}} = M_s/s$, and the effective anisotropy follows as $K = 0.5 \times \mu_0 M_s^2/s$. Our example gives $K = 57.8$ kJ m^{-3} [47].

This method is appealing for systems where the magnetoelastic coupling is measured by a reorientation of the sample magnetization; see section 2.5. As shown in figure 4, magnetic fields along two perpendicular directions are available for the magnetoelastic measurements, and the in-plane anisotropy can be derived. Combined MOKE and curvature measurements are a necessity to assure that the curvature measurements are performed for fully saturated magnetization states.

Table 1 summarizes the anisotropy constants of Fe, Co, and Ni, and the Curie temperatures. The values indicate a typical order of magnitude of a few μeV for the anisotropy energy per atom. The Curie temperatures indicate that the energy scale which characterizes the large scale ferromagnetic order is at least four orders of magnitude larger compared to the small energy scale which describes the energy dependence of the orientation of the magnetization in a crystalline lattice. Anisotropy measurements reveal a pronounced

Table 1. Magnetocrystalline anisotropy of bulk elements at the indicated temperature and Curie temperature [48]. Note that the meaning of K_1 depends on the crystal symmetry. Cubic: $K = K_1 S + K_2 P$, with $S = \alpha_1^2\alpha_2^2 + \alpha_2^2\alpha_3^2 + \alpha_1^2\alpha_3^2$, $P = \alpha_1^2\alpha_2^2\alpha_3^2$; hexagonal: $K = K_1 \sin^2\theta + K_2 \sin^4\theta$. K: magnetic anisotropy energy density; α_i: direction cosine with respect to the cubic axis i; θ: angle between c-axis and magnetization direction.

		bcc-Fe 273 K	hcp-Co 275 K	fcc-Ni 296 K
K_1	(MJ m^{-3})	0.048	0.513	−0.006
	(meV/atom)	0.0035	0.035	−0.0004
K_2	(MJ m^{-3})	0.001	0.001	−0.003
	(meV/atom)	0.000 07	0.000 07	−0.0002
T_C	(K)	1044	1360	627
	(meV/atom)	90	117	54

temperature dependence of these values, where the magnitude and sign of the constants can change with temperature [25, 48, 49].

The small magnitude of the magnetocrystalline anisotropy energy density, of order μeV, is challenging even for today's first principles calculations of the magnetic anisotropy. Nevertheless, recent state of the art calculations deliver reliable anisotropy data for many systems [50, 51]. The reader is referred to [17] for a compilation of recent work.

2.3. The magnetic anisotropy of ultrathin films

In sharp contrast to the small crystalline anisotropy of bulk samples, as indicated in table 1, ultrathin films often exhibit an effective magnetic anisotropy which is orders of magnitude larger than the respective bulk value. The deviation from the respective bulk values has been ascribed in most cases to a magnetocrystalline surface anisotropy of the Néel type. We refer to the extensive literature for a compilation of respective data [13, 52].

Films are generally idealized as perfectly flat extended ferromagnetic layers. Structural investigations indicate, however, that films are rough in general, and the impact of film roughness on the magnetic anisotropy of dipolar origin is discussed in section 2.9.1.

The substrates for film growth are also far from perfectly flat. Steps of often monoatomic height separate atomically flat terraces. If the sample surface is cut under same misorientation, then the average terrace size can be varied, and these vicinal substrates will induce film growth with a large density of steps. Depending on the system, an easy magnetization direction along the step edge, or perpendicular to the step edge, is observed [53–55]. Step atoms, like surface atoms, are characterized by a reduced coordination as compared to both bulk atoms and terrace atoms. Thus, according to the Néel model, an additional source of anisotropy is expected due to steps [18, 56]. This step anisotropy is a uniaxial contribution to the magnetic anisotropy. A calculation within Néel's model suggests that the surface anisotropy is always reduced by roughness, $\frac{\Delta K_S}{K_S} = -\frac{2\sigma}{\xi}$ [18, 56]. Here, σ denotes the mean vertical deviation from a reference plane, and ξ is the average lateral size of flat areas.

The assignment of a large anisotropy in ultrathin films to a surface effect neglects the impact of a film strain variation on the effective magnetic anisotropy. In many cases, films are epitaxially strained, and this film strain contributes via the magnetoelastic coupling to the anisotropy. With increasing thickness, misfit dislocations are formed, and the film strain changes with thickness, as does the magnetoelastic contribution to the magnetic anisotropy. This aspect is discussed in more detail in section 2.8 below.

2.4. Magnetoelastic anisotropy

The coupling between magnetism and lattice strain is a well known experimental fact, known as magnetostriction for bulk samples [57]. A sample lowers its total energy upon magnetization by a lattice strain, which depends on the magnetization direction with respect to the crystalline lattice. The underlying principle of the so-called magnetoelastic coupling can be described as the strain dependence of the magnetic anisotropy energy density [50]. This coupling between lattice strain and magnetic anisotropy is decisive for the magnetic properties of epitaxially strained ultrathin films.

Films, and also nanostructures, are in general under considerable strain, which often determines the magnetic anisotropy. A famous example is the out-of-plane easy magnetization direction over an extended thickness range from 10–50 atomic layers Ni on Cu(001), which is ascribed to the epitaxial strain of the Ni film [25, 58, 59].

Magnetoelastic coupling coefficients are directly accessible for an experimental determination. One exploits the change of the magnetoelastic stress in a film which is induced upon a magnetization reversal. This stress change is measured directly from the resulting curvature of a thin substrate [26, 60], as discussed next.

2.5. Magnetoelastic stress and film stress measurements

Cantilever bending experiments, as shown schematically in figure 4, are sensitive and accurate tools for the measurement of mechanical stress in atomic layers and at surfaces [63]. The idea of the measurement is to detect the stress-induced change of curvature of a thin ($\approx$100 μm) cantilever substrate. The curvature change is directly proportional to the film stress, integrated over the film thickness. The method reaches a sensitivity for the detection of adsorbate-induced surface-stress changes down to a coverage of 0.001 atomic layers, and for magnetoelastic stress measurements down to a few atomic layers thin films. See [26, 27, 60, 62, 64, 65] for a review of the technique and for the discussion of the quantitative curvature analysis.

Here we restrict the description to the essence of the analysis, i.e. the film stress τ is given by the slope of the curve of the curvature, plotted as a function of the film thickness [26]. The relation between film stress τ_i and curvature change $1/R_i$ is given for elastic isotropic substrates by

$$\begin{aligned}\tau_i &= \frac{Y_\mathrm{s}\, t_\mathrm{s}^2}{6\,(1-\nu_\mathrm{s})t_\mathrm{f}}\left(\frac{1}{R_i}+\nu_\mathrm{s}\frac{1}{R_j}\right)\\ \tau_j &= \frac{Y_\mathrm{s}\, t_\mathrm{s}^2}{6\,(1-\nu_\mathrm{s})t_\mathrm{f}}\left(\frac{1}{R_j}+\nu_\mathrm{s}\frac{1}{R_i}\right),\end{aligned} \tag{1}$$

where $i, j = x_1, x_2$ are directions along the sample length and width, respectively [26]. The substrate and film thickness are given by t_s and t_f, respectively. The elastic properties of the substrate are given by the Young's modulus Y_s and the Poisson ratio ν_s for the appropriate substrate orientation [26, 66]. Examples for the resulting curves of film stress versus film thickness are presented in figure 5.

The magnetoelastic coupling coefficients B_i are derived from the change of curvature which is measured during an in-plane reorientation of the film magnetization, as indicated in figures 4 and 2. The relation between the curvature change due to magnetization reversal from magnetization along the sample length $(1/R_x)^{\mathrm{length}}$ to magnetization along the sample width $(1/R_x)^{\mathrm{width}}$ and the effective magnetoelastic coupling B_eff is given by [26, 65]

$$B^{\mathrm{eff}} = \frac{Y_\mathrm{s}\, t_\mathrm{s}^2}{6\,(1+\nu_\mathrm{s})t_\mathrm{f}}\left(\left(\frac{1}{R_x}\right)^{\mathrm{length}} - \left(\frac{1}{R_x}\right)^{\mathrm{width}}\right). \tag{2}$$

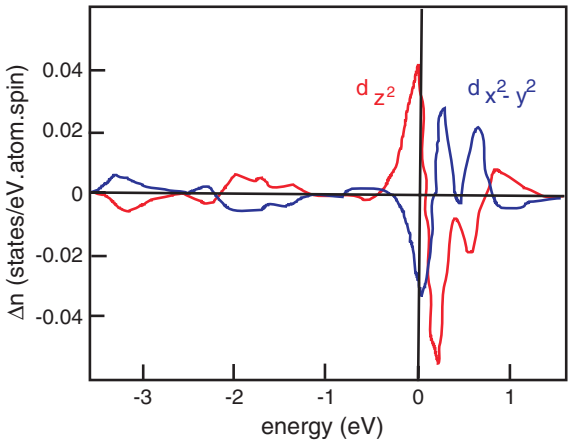

Figure 3. Calculated change of electron density of the 3d-states of bulk Fe, due to a compression along the z-axis. A net charge transfer from the $d_{x^2-y^2}$-state to the d_{z^2}-state is calculated. This induces an easy magnetization direction along the in-plane x–y-plane [38].

Table 2. Effective magnetoelastic coupling coefficients B_{eff} as determined from an in-plane magnetization reversal of a film with the given orientation and symmetry. The B_i are defined in equation (6). x_1: sample length; x_2: sample width. See [65] for details.

Film structure	B_{eff}
Cubic, film axes along x_1, x_2	B_1
Hexagonal, c-axis $\perp$ film plane	B_1
Cubic, film axes rotated by 45° with respect to x_1, x_2	B_2
Hexagonal, c-axis in-plane, 2 domains $\parallel x_1, x_2$	$\frac{1}{2}(B_1 - B_2 + B_3)$
Hexagonal, c-axis in-plane, 2 domains rotated by 45° with respect to x_1, x_2	B_4
Hexagonal, c-axis in-plane, 3 domains rotated by 120° with respect to x_1, x_2	$\frac{1}{4}(B_1 - B_2 + B_3) + \frac{1}{2}B_4$

Table 2 gives the proper magnetization and curvature measurement directions for the detection of the respective B_i [65].

The strength of the cantilever curvature method is the *i*n situ measurement of both film stress during film growth and of magnetoelastic stress on the identical film. These combined measurements have been applied to deduce the significant modification of the magnetoelastic coupling B_i by even a small lattice strain. Results of these measurements are discussed in section 2.8.

Ab initio based calculations on the magnetoelastic properties are a formidable task, as the relevant energy scales are so small, e.g. (sub)-μeV/atom [51, 67]. In these calculations, one either tries to derive the magnetization-induced lattice distortion directly [67], or one explores the strain dependence of the magnetic anisotropy [50, 68–72]. These calculations indicate that the lattice strain itself affects the magnitude of the magnetoelastic coupling, i.e. the coupling coefficients are strain dependent [68]. Both theory and experiment have shown that the respective bulk magnetoelastic coupling coefficients are not appropriate for the description of strained films [26].

Ab initio calculations offer the physical origin of the strain dependence of the magnetocrystalline anisotropy. Figure 3 shows the change of the orbital occupancy due to a tetragonal strain. The calculation indicates an electronic charge transfer from the $d_{x^2-y^2}$-state to the d_{z^2}-state upon a compression along the z-axis [38, 50], which in turn favours the in-plane magnetization over the out-of-plane magnetization direction.

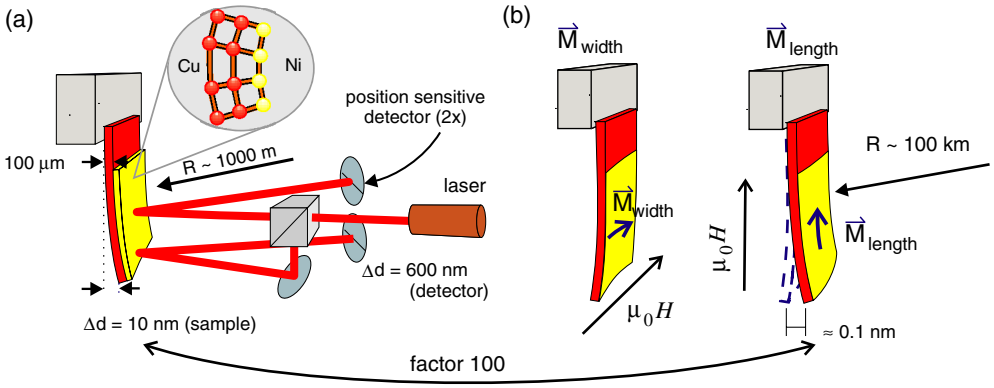

Figure 4. The cantilever technique for quantitative stress measurements during film growth (a) and magnetization processes (b). The stress-induced curvature of a thin (≈100 μm) cantilever sample is detected by an optical deflection technique, as described in [61, 62]. A switching of the film magnetization between two well defined directions allows us to extract the respective magnetoelastic coupling coefficients. Magnetoelastic stress is typically two to three orders of magnitude smaller than epitaxial film stress, which can be as large as several GPa.

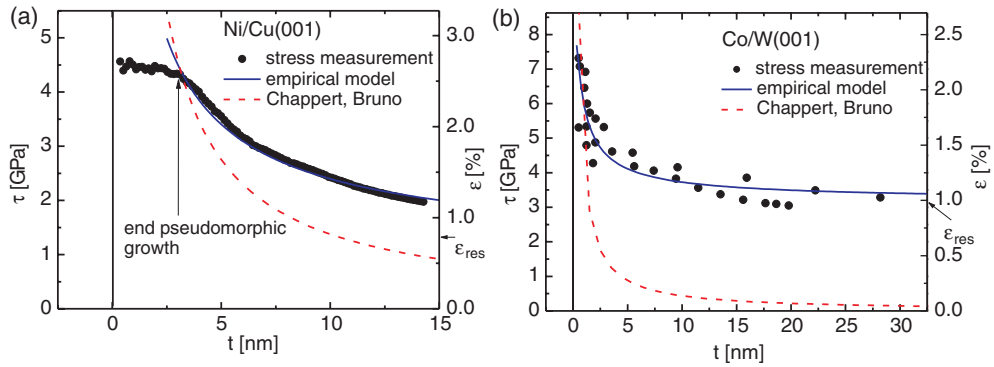

Figure 5. Stress measurements during the deposition of (a) Ni on Cu(001), and (b) Co on W(001), with deposition temperature 300 K. The critical thickness for the end of pseudomorphic growth is 3 nm for Ni, and 0.6 nm for Co. The Chappert–Bruno model of equation (3) gives a strain decrease, which is too strong compared to the data. The empirical model of equation (4) gives a satisfactory description.

In the following we introduce first in sections 2.6 and 2.7 the relations which describe the three-dimensional strain state. Then we elucidate in section 2.8 how these distortions couple to the magnetoelastic anisotropy contribution.

2.6. Lattice strain in epitaxial systems

The epitaxial growth of a material on top of a substrate leads in most cases to some misfit-induced strain at the interface between the deposit and the substrate. With respect to the film material, this corresponds to a strain $\eta = (a_{\mathrm{sub}} - a_{\mathrm{film}})/a_{\mathrm{film}}$. This misfit is determined by the lattice constants a_i, which describe the atomic distances on the relevant surface orientation. The misfit strain can be positive (tensile strain) or negative (compressive strain), and it can reach a magnitude of up to 10%. A larger misfit strain seems to inhibit pseudomorphic growth.

Table 3. Calculated out-of-plane strain ϵ_{33} for different film orientations, as a function of in-plane film strain ϵ_{11}, ϵ_{22}. The orientation of the film crystal axes is indicated. The elastic stiffness constants c_{ij} are tabulated [77, 78].

Cubic (100) 1 : [100], 2 : [010]	Cubic (110) 1 : [$\bar{1}$10], 2 : [001]	Cubic (111) 1 $\perp$ 2 : in-plane arbitrary	hcp (0001) 1 $\perp$ 2 : basal plane
$-\frac{c_{12}}{c_{11}}(\epsilon_{11}+\epsilon_{22})$	$-\frac{(c_{11}+c_{12}-2c_{44})(\epsilon_{11}+2c_{12}\epsilon_{22})}{(c_{11}+c_{12}+2c_{44})}$	$-\frac{(c_{11}+2c_{12}-2c_{44})}{(c_{11}+2c_{12}+4c_{44})}(\epsilon_{11}+\epsilon_{22})$	$-\frac{c_{13}}{c_{33}}(\epsilon_{11}+\epsilon_{22})$

The in-plane epitaxial misfit strain can be reduced by a rotation of the crystallographic unit cell of the film with respect to the substrate [73]. An example is the growth of Ag on Fe(001), where fcc-Ag grows with its (100) orientation on the bcc(100) face. The film crystal axes are rotated by 45° with respect to the bcc(100) axes, and a small compressive misfit of -0.8% results [74]. A reasonable epitaxial match between film and substrate can also be realized by the deposition of fcc(111) films on top of bcc(110) substrates, as for example in the case of Ni(111) films deposited on W(110) [75]. This example is discussed in view of its magnetic anisotropy in section 5.

The epitaxial misfit for simple epitaxial relations leads to an isotropic in-plane strain, i.e. $\epsilon_{11} = \epsilon_{22} = \eta$, and in other cases the in-plane film strain is anisotropic $\epsilon_{11} \neq \epsilon_{22}$. An anisotropic film strain is also generally expected for simple epitaxial systems like Fe/W(100), after misfit dislocations have been formed. Misfit dislocations are often formed along one preferential direction, which induces a uniaxial strain anisotropy, as will be shown in section 6.

Note that continuum elasticity predicts an out-of-plane strain ϵ_{33} as a result of the in-plane strain. For cubic materials this leads to a tetragonal distortion of the lattice, which has considerable impact on the magnetic anisotropy. This distortion reflects the Poisson-type reaction of the lattice upon an anisotropic strain. The magnitude of the resulting strain ϵ_{33} is calculated from the elastic energy density f_{elast} in the continuum elasticity description, from the requirement of a vanishing stress along the film normal, i.e. $\tau_{33} = \partial f_{\text{elast}}/\partial\epsilon_{33} = 0$. Table 3 gives the proper expressions for the out-of-plane strain for various crystallographic orientations, as a function of the in-plane strains. The corresponding change of the atomic volume is given by the trace of the strain tensor $\Delta V/V = (\epsilon_{11} + \epsilon_{22} + \epsilon_{33})$.

Highly sensitive diffraction studies by low-energy electron diffraction (LEED) on pseudomorphically strained Ni layers on Cu(100) confirm that continuum elasticity gives an appropriate description of the tetragonal distortion even in thin (a few atomic layers) films [76].

2.7. Film thickness dependent strain

It has been realized from the early studies of film growth that film strain varies with film thickness, for films which are thicker than the critical thickness t_c. Below t_c, the film strain ϵ is given by the epitaxial misfit η as determined by the lattice mismatch between film and substrate (see the discussion above in section 2.6), and ϵ is a constant. Above t_c misfit dislocations are formed, and the magnitude of the film strain decays with increasing film thickness [64, 79–82].

Chappert and Bruno have extracted the following approximate relation for the thickness dependence of the film strain [83]:

$$\epsilon(t) = \eta\, t_c/t; \tag{3}$$

this expression is now in wide use when it comes to the discussion of strain effects for magnetic anisotropy [22]. But how well does equation (3) describe the experimental results?

It can be safely assumed that any variation of the strain ϵ of a film will also induce a corresponding change of the film stress τ, as the two quantities are coupled together via

elasticity relations. For an isotropic biaxial strain this relation is given by $\tau = \epsilon\, Y/(1-\nu)$, where Y and ν are the Young's modulus and Poisson's ratio, respectively, of the film [26]. Therefore we discuss in the following the thickness dependence of the measured film stress, and discuss the result in view of strain-decay models.

In contrast to the result of equation (3), experiments as shown in figure 5 indicate that the film strain decays more weakly as a function of thickness. As already pointed out by Matthews and Crawford [79], the experimentally observed strain above t_c is for numerous systems substantially higher than the calculated value from different strain models.

From many stress measurements performed on different epitaxial systems we find a considerable residual strain, even in rather thick films. Up to a film thickness of 70 nm, we find that the film strain approaches a residual strain level of the order of 0.3–1% [26, 84, 85]. Therefore, an inclusion of the residual strain in the description of the thickness dependence of film strain seems appropriate [85], and this aspect is missing in equation (3).

We note in passing that experimental stress curves can often be adequately described by the following empirical expression [85], which is based on the work of Matthews and Crawford [79], and which takes a residual stress into account:

$$\tau(t) = \frac{\alpha}{t}\,\ln\left(\frac{\mathrm{e}}{b}\,t\right) + \tau_{\mathrm{res}}, \tag{4}$$

where b is the Burger's vector (for Ni(100): $b = 0.25$ nm), and α and τ_{res} are fit parameters. This relation leads to a weaker stress decrease with increasing thickness, and it describes the experimental situation satisfactorily (see figure 5), in contrast to equation (3).

The validity of certain strain-decay models as quoted above should be viewed with caution. The introduction of misfit dislocations, and the corresponding structural changes, are strongly temperature dependent. Therefore, one cannot expect that a single relation gives an appropriate description of the film strain above the critical thickness. Our examples show that a simple $1/t$ dependence is certainly not appropriate in general. This questions the common practice, to discuss strain-related magnetic anisotropy for $t > t_c$ in terms of surface contributions to the anisotropy, simply due to the falsely assumed $1/t$-strain variation with thickness.

Recent surface x-ray diffraction studies confirm that sizeable strains in the per cent range are still present in $\approx$10 layer thick Fe and Ni films on W(110). These studies also prove the crucial dependence of the film strain on, for example, the growth temperature [75, 86, 87]. Therefore we conclude with the assertion that structural investigations are mandatory to quantify film strain reliably.

An important result of the stress measurements is that even thicker films are under some considerable strain, and for films up to a thickness of several tens of nanometers a residual strain has to be considered. This has important consequences for the magnetic anisotropy, as discussed next.

2.8. The magnetoelastic anisotropy of ultrathin films

The magnetoelastic coupling coefficients B_i couple the strain ϵ_{ij} to the magnetoelastic magnetic anisotropy energy density f_{me}. The following expressions describe the magnetoelastic coupling in cubic and hexagonal systems, respectively [26, 65]:

$$\begin{aligned} f_{\mathrm{me}}^{\mathrm{cubic}} &= B_1(\epsilon_{11}\alpha_1^2 + \epsilon_{22}\alpha_2^2 + \epsilon_{33}\alpha_3^2) \\ &\quad + B_2(2\epsilon_{12}\alpha_1\alpha_2 + 2\epsilon_{23}\alpha_2\alpha_3 + 2\epsilon_{23}\alpha_2\alpha_3) + \cdots \end{aligned} \tag{5}$$

$$\begin{aligned} f_{\mathrm{me}}^{\mathrm{hex}} &= B_1(\epsilon_{11}\alpha_1^2 + 2\epsilon_{12}\alpha_1\alpha_2 + \epsilon_{22}\alpha_2^2) \\ &\quad + B_2(1-\alpha_3^2)\epsilon_{33} + B_3(1-\alpha_3^2)(\epsilon_{11}+\epsilon_{22}) \\ &\quad + B_4(2\epsilon_{23}\alpha_2\alpha_3 + 2\epsilon_{13}\alpha_1\alpha_3) + \cdots. \end{aligned} \tag{6}$$

Table 4. Magnetoelastic coupling coefficients in MJ m^{-3} at room temperature [26, 88].

	bcc-Fe	hcp-Co	fcc-Ni
B_1	−3.43	−8.1	9.38
B_2	7.83	−29.0	10.0
B_3		28.2	
B_4		37.5	

Table 5. Contribution of the magnetoelastic anisotropy f_{me} to the magnetic anisotropy energy density for in-plane film strain $\epsilon_{11} = \epsilon_{22} = \epsilon_0$, and out-of-plane strain ϵ_3, for different film orientations, and different magnetization directions [89].

Film surface and magnetization directions	f_{me}
Cubic(001), in-plane, all directions	0
Cubic(001), out-of-plane [100]–[001]	$B_1(\epsilon_0 - \epsilon_3)$
Cubic(110), in-plane [100]–[$\bar{1}$10]	$0.5(B_2 - B_1)(\epsilon_0 - \epsilon_3)$
Cubic(110), out-of-plane [$\bar{1}$10]–[110]	$B_2(\epsilon_0 - \epsilon_3)$
Cubic(111), in-plane, all directions	0
Cubic(111), out-of-plane	$B_2(\epsilon_0 - \epsilon_3)$
Hexagonal(0001), in-plane, all directions	0
Hexagonal(0001), out-of-plane	$(B_1 + 2B_3)\epsilon_0 + B_2\epsilon_3$

The α_i are the direction cosines of the magnetization direction with respect to the crystalline axes. The dots indicate that we have omitted higher order contributions in strain ϵ for clarity. However, these contributions are decisive for epitaxially strained systems discussed below, as they induce the experimentally found dependence of B on lattice strain, i.e. $B = B(\epsilon)$.

Table 4 gives the bulk values B_i for bcc-Fe, hcp-Co and fcc-Ni. Note the orders of magnitude larger values as compared to the magnetocrystalline anisotropy constants quoted in table 1. Strains in the per cent range induce via the magnetoelastic coupling significant contributions to the magnetic anisotropy.

Epitaxial strain leads in general to a reduced symmetry of the film, as compared to its unstrained bulk counterpart. Table 5 gives the relations which describe the resulting magnetoelastic contribution to the magnetic anisotropy, as induced by an anisotropic strain, for cubic and hexagonal systems.

The experimental determination of the magnetoelastic coupling coefficients has shown that film strain modifies the magnetoelastic coupling considerably [26, 60]. The sign and magnitude of the respective coupling coefficients depend on the lattice strain.

Table 6 summarizes the experimental results from several studies on the strain-dependent magnetoelastic coupling [27]. These data are based on combined film stress and magnetoelastic stress measurement, as described in section 2.5, figure 4. Thus, film stress, film thickness, and magnetoelastic coupling coefficients are determined in experiments. The film strain is then calculated from the measured stress by continuum elasticity.

We conclude the discussion of magnetoelastic anisotropy by an application of the strain-modified B_i to the discussion of the in-plane anisotropy of Fe(110) on W(110). This is a prototype system, where the deviation of the film anisotropy form the bulk behaviour has been studied extensively [44].

Thin Fe films on W(110) have an easy in-plane magnetization direction along [$\bar{1}$10], which reverts to the easy bulk direction, in-plane [001], for a thickness in excess of approximately 50 layers. This in-plane anisotropy has been ascribed to a surface anisotropy contribution to the magnetic anisotropy [44], but here we want to elucidate to what extent the misfit strain-induced magnetoelastic anisotropy can be held responsible for the in-plane anisotropy [89].

Table 6. Strain-modified magnetoelastic coupling coefficients at room temperature. Experimental data obtained from cantilever bending measurements on epitaxial films. The in-plane film strain ϵ modifies the respective bulk value B_i.

	B_i^{eff} (MJ m^{-3})	Strain correction	References
Fe	B_1^{eff}	$-3.0 + 1000\,\epsilon$	[26]
		$-3.4 + 1041\,\epsilon$	[60][a]
	B_2^{eff}	$+7.5 - 360\,\epsilon$	[60][a]
Ni	B_1^{eff}	$+9.4 - 234\,\epsilon$	[88]
Co	B_4^{eff}	$+3.4 + 1346\,\epsilon$	[90][b]

[a] Data were taken for different stress τ. Conversion $\tau = 208\,\epsilon$ [26]. The original data imply that a linear correction of B_1 for Fe is only found for stress <1 GPa, or strain <0.01. For larger values B_1 remains at 1–2 MJ m^{-3} [26, 60].

[b] The film structure is comparable to dhcp, therefore the reference for the constant value is not B_4^{hcp}, but rather $B_4^{\text{dhcp}} \approx 6$ MJ m^{-3} [90].

Our structural investigation by surface x-ray diffraction of 13 layers of Fe on W(110) identifies an in-plane film strain $\epsilon_{11} = \epsilon_{22} = 0.012$, and out-of-plane $\epsilon_3 = 0.0022$ [86]. The measured film stress is isotropic and amounts to 13 GPa [26]. We refer to the stress-dependent B_i measurements [60], and extract $B_1(13\,\text{GPa}) \approx 2$ MJ m^{-3}, and $B_2(13\,\text{GPa}) \approx -15$ MJ m^{-3}. The magnetoelastic contribution to the in-plane anisotropy results as $0.5(B_2 - B_1)(\epsilon_{11} - \epsilon_{33}) = -0.08$ MJ m^{-3}. This value compares reasonably well with the value of -0.11 MJ m^{-3}, calculated for 13 layers of Fe from the anisotropy study of Elmers and Gradmann [44]. We conclude that the strain-dependent magnetoelastic anisotropy is sufficient to induce the in-plane anisotropy of strained Fe(110) films. There is no need to introduce significant surface anisotropy terms to explain the non-bulk-like magnetic anisotropy. With increasing thickness, a further relaxation of film stress and strain is expected, and this will also induce an in-plane SRT to the easy bulk magnetization direction [001].

This result suggests that we should reconsider if an SRT at a thickness well above the critical film thickness might be due to a strain-dependent magnetoelastic coupling, and not necessarily to a magnetic surface anisotropy. This statement does by no means imply that the magnetic surface anisotropy is a questionable concept in general. Indeed, we will see in section 5 that for example an adsorbate layer can induce an SRT without inducing a significant change of strain. This underlines the significance of magnetic surface anisotropy in situations where the *surface* of a ferromagnetic layer is modified. However, when the variation of film strain enters the discussion of magnetic anisotropy, clearly bulk effects come into play. A discussion in terms of surface anisotropy disguises the physical origin of this strain-induced SRT.

2.9. Shape anisotropy

The magnetization of a sample induces a magnetic stray field in its surroundings. The energy cost of such a stray field depends on the shape of the sample, and on the orientation of the magnetization with respect to the sample shape. A limiting case is the continuous flat film, which produces a stray field energy density, the so-called shape anisotropy, of $\frac{1}{2}\mu_0 M_s^2$ for a magnetization perpendicular to the film plane. For in-plane magnetization, the stray field energy is zero. The shape anisotropy is of dipolar origin. It is usually calculated from a continuous magnetization of the sample. This is, however, an approximation. The discrete nature of magnetization, and the symmetry of the arrangement of magnetic moments, lead to corrections for the shape anisotropy of nanoplatelets. This effect is discussed in section 2.9.2.

Table 7. Spontaneous magnetization M_s and shape anisotropy for out-of-plane magnetization at the indicated temperature [48].

		bcc-Fe 286 K	hcp-Co 287 K	fcc-Ni 287 K
M_s	(kA m^{-1})	1717	1447	493
$\mu_0 M_s$	(T)	2.16	1.82	0.62
$\frac{1}{2}\mu_0 M_s^2$	(MJ m^{-3})	1.85	1.32	0.15
	(meV/atom)	0.14	0.09	0.012

Table 7 gives the magnetization and the shape anisotropy for out-of-plane magnetization for Fe, Co and Ni. Note that the shape anisotropy scales with the square of the magnetization. An out-of-plane magnetization of Ni gives rise to a shape anisotropy which is roughly an order of magnitude smaller as compared to an Fe film of the same thickness.

2.9.1. The shape anisotropy of rough films and of islands. Film growth is in general classified into three growth modes: (i) Frank–van der Merwe (layer-by-layer growth), (ii) Stranski–Krastanov (island growth on top of a flat film, which covers the substrate), and (iii) Vollmer–Weber (island growth) [73, 91–93]. One expects rather flat and smooth films for Frank–van der Merwe growth, whereas Vollmer–Weber growth leads to rough surfaces. The film roughness, as given for example by the ratio between the average vertical height variation σ and the lateral correlation length ξ, induces an important contribution to the magnetic anisotropy [56, 94], as will be apparent from the following discussion.

Even film–substrate combinations which are described as layer-by-layer systems show some roughness, especially for larger thickness, as evidenced by scanning tunnelling microscopy or medium energy electron diffraction studies [28, 92, 93, 95], and a usually small variation of the dipolar shape anisotropy is induced.

Bruno [94] pointed out that a stray-field contribution to the magnetic anisotropy has to be considered for in-plane magnetization of rough films. In contrast to perfectly flat films, where the in-plane magnetization does not lead to any stray field for large film areas, a stray field is due to the in-plane magnetization of rough films. An important consequence is that the difference between the stray field energy density for magnetization along the surface normal as compared to magnetization in the film plane is reduced. The out-of-plane magnetization becomes energetically favourable for a rough film.

According to Bruno [94], the film roughness is described by two parameters: σ, the average height deviation from a reference plane, and ξ, the average lateral size of flat areas. The reference plane is chosen such that the film has its nominal thickness t. The calculation shows that the stray field energy for perpendicular magnetization of a rough film, $E_\perp^{\text{rough}}$, is reduced: $E_\perp^{\text{rough}} = 0.5\mu_0 M_s^2\, t(1 - \frac{\sigma}{2t}(1 - f(\sigma/\xi)))$. The function f has the value 1 for a flat film, $\sigma = 0$, and it approaches 0 for increasing roughness, $\sigma/\xi \to 1$.

This model shows that film roughness gives rise to a small dipolar surface anisotropy contribution of magnitude $\sim\sigma/t$. This roughness-induced dipolar anisotropy has been estimated to be never sufficient to induce a spin reorientation transition (SRT) from in-plane to out-of-plane for a continuous film [94].

The Bruno model of the influence of roughness on the magnetic anisotropy has been applied in a combined scanning tunnelling microscopy (STM) and ferromagnetic resonance (FMR) study of Ni layers on Cu(001) [95]. This study confirmed the assertion that the roughness-induced change of the magnetic anisotropy is a small effect. In this study, film roughness

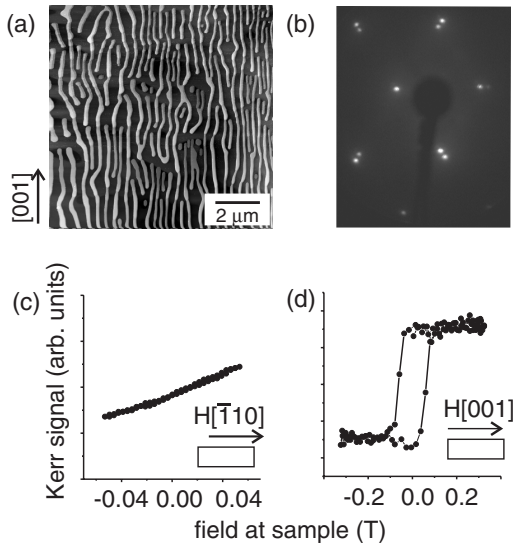

Figure 6. Fe island formation upon annealing of an Fe film, deposited on W(110) at 300 K [26]. (a) The STM image shows elongated Fe islands (height 17 nm), oriented along [001]. (b) The LEED pattern shows two sets of bcc(110) diffraction spots, indicative of bulk Fe- and W-lattice constants. (c) and (d) MOKE measurements of an annealed Fe film with magnetization along [$\bar{1}$10], and [001]. The easy axis is [001]. The MOKE curves of the as-grown film are shown in figure 1, where the easy magnetization direction is [$\bar{1}$10].

has moved the critical thickness, above which an easy out-of-plane magnetization is observed, by one atomic layer. Roughness favours an out-of-plane easy magnetization direction, in accordance with the model.

The consideration of in-plane demagnetizing fields extends to the discussion of magnetic in-plane anisotropy of elongated structures. Such structures can be produced in a self-organized way by annealing a film at higher temperatures, or by choosing the growth parameters accordingly. For these structure one expects a magnetic shape anisotropy which favours a magnetization along the long axis, as this keeps the stray field energy low. The impact of the island shape on the magnetic anisotropy is discussed next.

We conclude the discussion of the magnetic shape anisotropy with an example regarding the in-plane magnetic anisotropy of elongated Fe islands with lengths in the several micrometres range, and widths of roughly 100 nm [96–98]; see figure 6.

Figure 6 shows an STM-image (a) and the corresponding LEED pattern (b) of the Fe island structure, which is prepared by Fe evaporation at 300 K, followed by annealing at 700 K for several minutes. The LEED pattern indicates two sets of bcc(110)-diffraction spots, which indicate bulk Fe- and W-lattice constants. The epitaxial strain due to the lattice misfit of 10% between Fe and W is completely relaxed in the Fe islands. Both island formation and strain relaxation lead to an easy magnetization direction along ⟨100⟩, as shown in the lower panel of figure 6.

In this example, the shape anisotropy promotes the same easy magnetization direction, and the question arises which effect, shape anisotropy or strain relaxation, is decisive [99] for the in-plane reorientation of the easy magnetization direction.

The discussion of magnetoelastic anisotropy in the next section will show that the lattice strain in the Fe/W system is sufficient to induce an in-plane easy magnetization direction

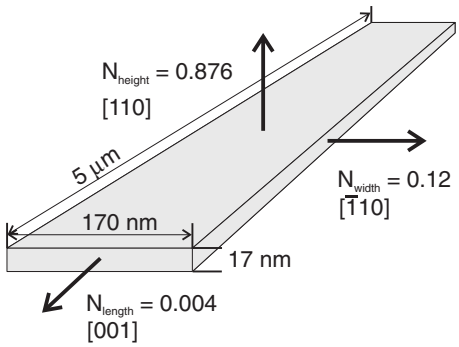

Figure 7. Sketch of an average Fe island on W(110) after annealing, as derived from the STM image of figure 6(a) above. The demagnetizing factors N_i for magnetization along the different directions as indicated by the arrows are calculated [100] for a length of 5 μm, width 170 nm, and height of 17 nm.

along $\langle 110 \rangle$. Consequently, strain relaxation upon island formation, as indicated by the LEED pattern, is an important factor for this in-plane spin-reorientation transition (SRT).

The shape anisotropy of the islands can be calculated by approximating the island shape with a rectangular prism of height 17 nm, width 170 nm, and length 5 μm, as suggested by the STM image of figure 6(a), and sketched in figure 7. The demagnetizing factors N_i are calculated from Aharoni's work [100], and are given in figure 7, and plotted for different aspect ratios in figure 8. The calculations indicate that the shape anisotropy $N_i \times 0.5\mu_0 M_s^2$ is almost negligible for magnetization along the length of the islands, and it is largest for magnetization along the film normal. But magnetization along the island width does also induce a sizeable shape anisotropy of 0.22 MJ m^{-3} (1.7 meV/atom), which favours a magnetization along [001] as compared to the in-plane [$\bar{1}$10] direction. In this example, the shape anisotropy is even larger in magnitude as compared to the magnetoelastic anisotropy induced by the strain relaxation, 0.08 MJ m^{-3} (see section 2.7), and both effects contribute to the in-plane SRT.

In figure 8 we present a compilation of calculated demagnetizing factors of rectangular samples for different length-to-width ratios. The plots indicate that the shape anisotropy of elongated islands depends on both the in-plane and the out-of-plane aspect ratio of the island. The in-plane anisotropy of elongated islands due to shape anisotropy is larger for thicker islands as compared to thinner islands.

Film roughness and island morphology are not only decisive for the shape anisotropy, they also determine the strain relaxation of these structures [101]. Stress measurements [27, 102] have clearly indicated that the strain in nanometer small islands is considerably relaxed as compared to extended islands [101]. In general one expects a pronounced strain relaxation in rough structures, e.g. in islands, as compared to extended flat structures, where strain relaxation is often hindered due to pseudomorphic growth. The effect of strain relaxation on the magnetic anisotropy is mediated by the magnetoelastic coupling, and it can be decisive due to the large magnitude of the respective coupling coefficients, as discussed in section 2.4.

2.9.2. The shape anisotropy of nanoplatelets. The calculation of the shape anisotropy has been performed for spheroidal or prismatic samples in the approximation of a continuum magnetization. The derived demagnetizing factors depend on a geometric ratio k, which is for example given by the thickness-to-diameter ratio t/L of the sample shape [7, 9, 100, 103]. These calculations were applied in section 2.9.1 above to discuss the shape anisotropy of elongated islands.

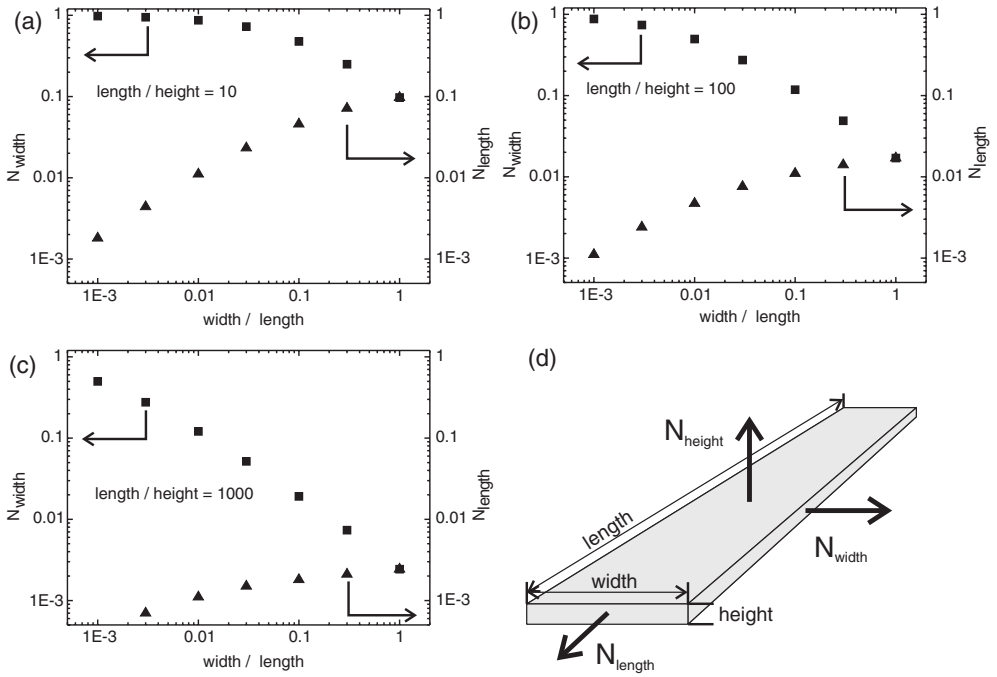

Figure 8. Calculated demagnetizing factors N_{width}, left-hand scales (squares) and N_{length}, right-hand scale (triangle), as a function of the width-to-length ratio of a rectangular sample, see (d). (a)–(c) Length-to-height ratio 10, 100, 1000. $N_{\text{height}} = 1 - N_{\text{width}} - N_{\text{length}}$.

It has been proposed that the model of a continuum magnetization is no longer valid when the film thickness is reduced to a few atomic layers [104]. In this case the system is treated as a collection of discrete magnetic dipoles, which are arranged on a crystalline lattice. Calculations of the shape anisotropy have been performed for infinite large ultrathin films, and a deviation from the continuum magnetization model was found for films thinner than 16 Å. The consideration of a discrete magnetization yielded a reduced stray field energy for perpendicular magnetization of ultrathin films as compared to thick films, and the magnitude of deviation depends on the lattice type [104].

Recent work on the numerical calculation of the shape anisotropy of structures with a limited lateral size [105, 106] goes beyond the previous findings in demonstrating for the first time that the magnetization direction can be changed by shrinking the lateral size, keeping the thickness fixed. The results of the earlier studies [104] are retrieved for the limiting case of infinite lateral structures. Analytical approximations of the results of the recent numerical calculation have been provided [107]. In an extension of the earlier work, noncollinear spin states due to thermal disorder have been considered, and the temperature-driven magnetic reorientation is discussed in view of the different temperature dependence of dipolar and magnetic anisotropy energies [105].

An important aspect of the recent calculation is that the shape anisotropy of discs with diameters of several hundred lattice constants and a few atomic layers thickness (nanoplatelets), depends on both size L and thickness t, and not just simply on the ratio of the two parameters. A remarkable result of the recent calculations is that the size effect already comes into play for rather large monolayer platelets of a few hundred atoms in diameter, and not only for situations where $L/t = 1$ [105, 106]. However, for the reasonably large island structure discussed above

and shown in figure 6, the deviations from the former continuum magnetization approach are negligible, but they become appreciable on smaller length scales.

What is a typical magnitude of the size-dependent stray field energy contribution to the magnetic anisotropy? A nanoplatelet with a diameter $L = 200$ atoms, and a thickness of one atomic layer, has a shape anisotropy of only $0.9 \times 0.5\mu_0 M_s^2$ [106]. The energy cost for perpendicular magnetization is reduced as compared to the full shape anisotropy $0.5\mu_0 M_s^2$, and the system might show an SRT from in-plane to out-of-plane magnetization. Such an SRT would be solely driven by the size-dependent shape anisotropy. In addition to the size of the platelet, the symmetry of the atomic arrangement also enters the calculation of the shape anisotropy on small length scales. Whereas the shape anisotropy of a triangular lattice is lower than that of the spheroid, a cubic atomic arrangement leads to a larger shape anisotropy as compared to the continuous spheroid [105, 106].

3. The experimental determination of magnetic anisotropy

Different experimental techniques are available to determine the magnetic anisotropy of ultrathin films and of nanostructures quantitatively. The magnetic anisotropy has a direct impact on the spin dynamics, and consequently ferromagnetic resonance experiments (FMR) [25, 108] and Brillouin light scattering (BLS) [109, 110] have been successfully applied to study magnetic anisotropy of ferromagnetic monolayers. The magnetic anisotropy also gives rise to a mechanical torque, when a magnetized sample is exposed to an external magnetic field. This mechanical torque acts as a directional moment in torsion oscillation magnetometry (TOM) [111], and numerous studies have been performed by TOM to obtain anisotropy information on a large variety of film–substrate combinations [13, 44].

FMR, BLS, and TOM are highly sophisticated techniques which require dedicated ultra-high vacuum (UHV) experiments for the appropriate measurement of the magnetic anisotropy, and further details can be found in the references cited above. In contrast to these techniques, magnetooptical Kerr-effect (MOKE) measurements have evolved into a well established technique [112], which characterize magnetic properties with sub-monolayer sensitivity. In MOKE experiments one exploits the magnetooptical response upon reflection of polarized light from a ferromagnetic sample. The polarization, the ellipticity and the intensity of the reflected light depend upon the magnetization direction of the sample with respect to the optical plane of the experiment. Thus, a variation of the magnetization of the sample in a magnetizing field gives rise to a corresponding change of these properties. A signal in proportion to the magnetization is obtained, but due to the magnetooptical nature of the experiments, absolute values of the sample magnetization cannot be extracted. However, the relative magnitude of the sample magnetization M with respect to the saturation M_s is accessible in cases where a saturation magnetization is obtained in the magnetization cycle. This is sufficient to deduce quantitative values for the magnetic anisotropy, as discussed next.

3.1. The magnetic circular dichroism of magnetic structures

Magnetic circular dichroism in x-ray absorption (XMCD) [41, 113] is a technique which offers elemental specific information on the magnetization. These measurements are performed at the L_3 (e.g. L_3(Co) = 779 eV) and L_2 (e.g. L_2(Co) = 794 eV) absorption edges of the magnetic materials, and the magnetization of the sample can be extracted from the peak intensity at the absorption edge, measured as a function of magnetization [41]. The measurements also allow a quantitative discussion of the contribution of spin and orbital moments to the

magnetization, and this makes XMCD a powerful tool to investigate the electronic origin of the magnetic anisotropy. Synchrotrons are required as highly brilliant light sources to obtain a sufficiently high photon flux at the energy of the absorption edges of ferromagnetic elements. XMCD gives an elementally-resolved magnetic characterization of multilayer structures [41], and it has a stunning sensitivity which allows one to study magnetism of low-dimensional atomic ensembles [114], down to individual atoms [43]. Recent measurements by XMCD have indicated a record high anisotropy of individual Co atoms of 9 meV/atom, and these experiments are discussed in section 7.

4. The temperature dependence of magnetization and magnetic anisotropy

Not only does the magnetic anisotropy of ultrathin films show dramatic deviations from the respective bulk value, but also the temperature dependent magnetization and anisotropy data indicate novel properties, which are characteristic of the reduced dimensionality of the ultrathin film environment. We present in the following two examples for the peculiar temperature dependence of both magnetization and anisotropy. This section gives a flavour of the peculiar temperature effect on the magnetic properties of atomic layers. The reader is referred to the review articles for a more complete compilation [23, 25, 28, 116, 117].

Surface sensitive magnetic measurements offer the opportunity to probe the magnetization in the surface region. Such experiments have been performed to study the magnetization near the Curie temperature. These experiments have indicated that the critical behaviour in 2D-systems like surfaces or atomic layers deviates distinctly from the respective bulk behaviour.

The Curie temperature of ultrathin films T_C depends on the film thickness. The Curie temperature T_C increases from 217 K for four layers of Ni on Cu(001) to 275 K at five layers, to 360 K at eight layers [118], which is still considerably smaller than the bulk value of 627 K. The decrease of T_C with decreasing film thickness is a general phenomenon, and a rule of thumb suggests a reduction of T_C from its bulk value in K by 50% in a five layer thin film. The observed thickness dependence can be reproduced by the thermodynamic description of the phase transition, with a critical exponent, which depends on the dimensionality of the system [28]. For Ni(111) layers, a dimensional crossover from a 2D- to a 3D-behaviour has been found to occur between five layers (2D) and seven layers (3D) [119].

Arnold and Pappas [115] have investigated whether T_C is different for the surface of a Gd film as compared to the bulk of the film. They employ spin-polarized electron-emission spectroscopy as a surface sensitive tool, and they take MOKE to study the bulk magnetization, as shown in figure 9. Their experiments show an identical T_C for both surface and bulk. However, near T_C, the magnetization of the surface decays faster as compared to the bulk. This is expressed by different critical exponents β, which describe the magnetization decay according to $M(T) = M_0(1-T/T_C)^{\beta}$, with $\beta_s = 0.88$, and $\beta_b = 0.376$. These values indicate a proper description of the magnetization of the Gd film as a 3D-Heisenberg magnet, which is physically appealing in view of the localized magnetization of Gd, with isotropic exchange coupling [115].

An unexpected phase transition with increasing temperature has been found by Farle *et al* [25, 120]. 8.2 layers Ni deposited on Cu(001) show an in-plane magnetization direction at low temperature, which reverts to out-of-plane around 185 K. This is indicated by the hard-axis magnetization loop for low temperature in figure 10(a), and by the remanent polar magnetization at higher T. This SRT is fully reversible upon temperature variations. A canted magnetization direction has been proposed for the intermediate temperature range. The resulting phase diagram is presented in figure 10(b). This temperature-driven SRT has

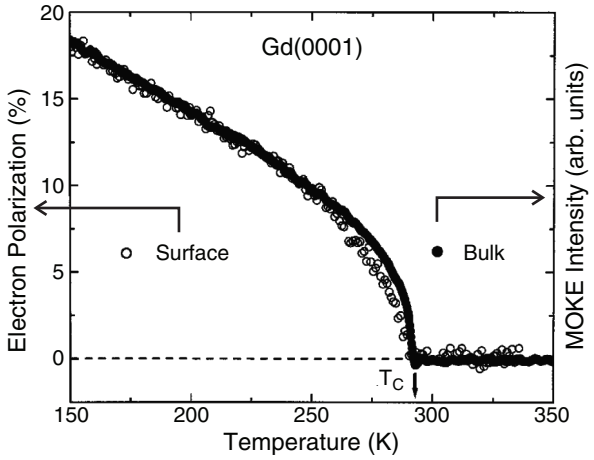

Figure 9. Surface magnetization (open symbols, electron polarization, left-hand scale), and bulk magnetization (filled symbols MOKE, right-hand scale) of a Gd film on W(110). The surface and bulk T_C coincide. The surface magnetization decays faster with approaching T_C, as compared to the bulk. From [115].

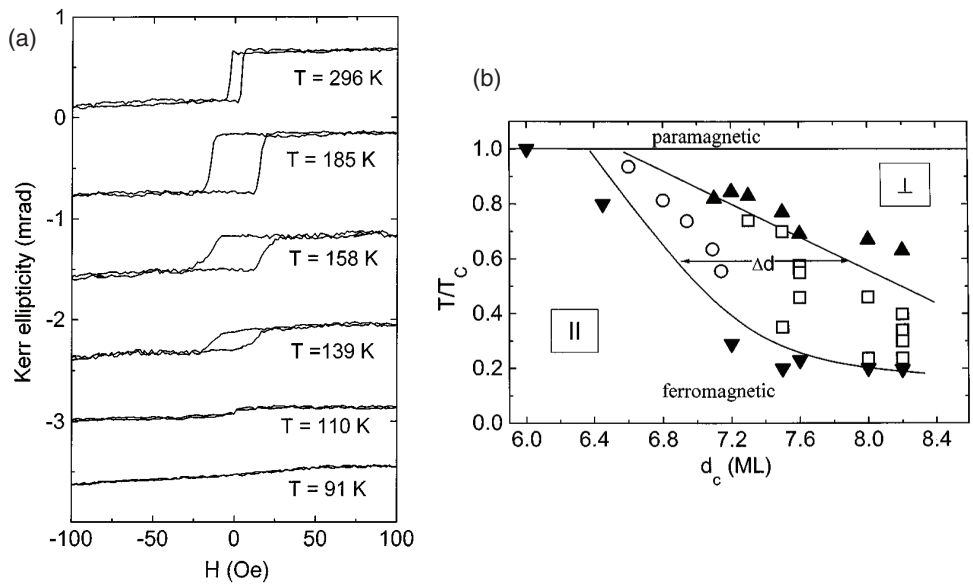

Figure 10. (a) Polar MOKE magnetization curves as a function of temperature for 8.2 layers Ni on Cu(001). A remanent polar magnetization emerges with increasing T. (b) Phase diagram for Ni layers on Cu(001). Two lines indicate a transition region, between easy magnetization in-plane $\parallel$, and out-of-plane $\perp$, where the magnetization is canted. T_C (8 layers) = 365 K. From [120].

been ascribed to the temperature dependence of the volume and surface anisotropy. The authors ascribe this SRT to a second order phase transition with a continuous change of the easy magnetization direction [120].

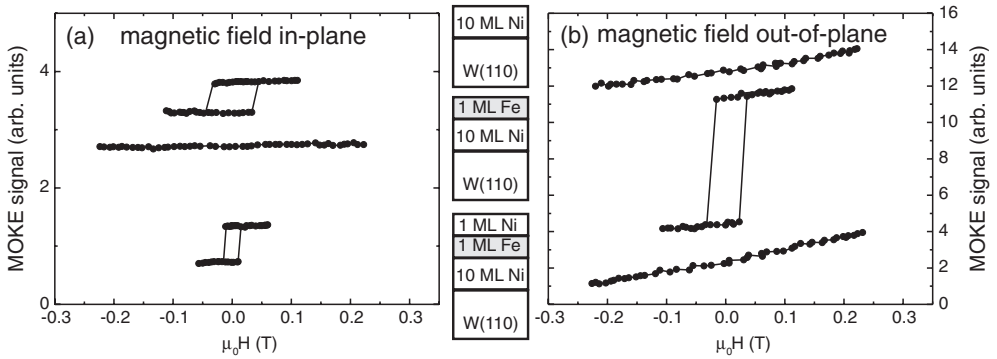

Figure 11. MOKE measurements of 10 atomic layers Ni(111), deposited on W(110). (a) Magnetizing field in-plane, (b) magnetizing field out-of-plane. Note how the coverage of the film by Fe, and subsequently by Ni, changes the magnetization curves from easy in-plane, to out-of-plane, and back to easy in-plane magnetization, respectively. The layer structure is indicated for the top, centre, and bottom curves. The magnetizing field was aligned in-plane along Ni[$\bar{1}$10], and out-of-plane along Ni[111].

5. The adsorbate-induced spin reorientation transition on ferromagnetic monolayers

Experimental and theoretical [40, 121] reports have identified the decisive role of an adsorbate coverage for the magnetic anisotropy of ferromagnetic layers. Examples are the Ag-, Au- and Cu-induced change of the in-plane anisotropy of Fe(110) layers [44], the H-induced reorientation of the easy magnetization direction of Ni monolayers to out-of-plane [59, 121], and the Fe-layer-induced easy magnetization direction of Ni(111) layers to out-of-plane [122]; see figure 11. Examples of other gas-induced SRTs are compiled in [123].

In this section we elucidate the role of possibly small adsorbate-induced structural relaxations for the adlayer-induced spin reorientation transition, i.e. we want to present experimental evidence for an upper limit of the adlayer-induced structural relaxation, and we discuss the corresponding influence on the magnetic anisotropy, as mediated by the magnetoelastic coupling.

As already pointed out in section 2.4, the large magnitude of the magnetoelastic coupling coefficients opens a way to influence the magnetic anisotropy by even subtle structural changes. Consider for example an adsorbate-induced easy out-of-plane magnetization. Obviously, the stray field energy density has to be compensated by the adlayer-induced change of magnetic anisotropy. For Ni layers, the stray field energy density is 0.01 meV/atom, as given in table 7. What amount of lattice strain is necessary to obtain a comparable anisotropy energy density? The answer is given by the magnetoelastic coupling coefficients. For a rough estimate we extract from table 4 an order of magnitude of $B \approx 0.68$ meV/atom. Thus, a variation of the perpendicular lattice strain by 1.5% is sufficient to induce a spin-reorientation transition.

A more rigorous treatment takes the epitaxial orientation and the anisotropy of the in-plane strain as compared to the out-of-plane strain into account, as elaborated in section 2.4, and given below for the case of Ni(111). Here it is sufficient to appreciate that strain variations in the per cent range have the potential to induce a spin reorientation transition. Thus experiments on the correlation between adsorbate-induced SRT and structural modifications seem worthwhile, and have been performed [87].

We combined MOKE measurements with surface x-ray diffraction experiments to correlate the adlayer-induced reorientation of the easy magnetization direction of Ni(111)

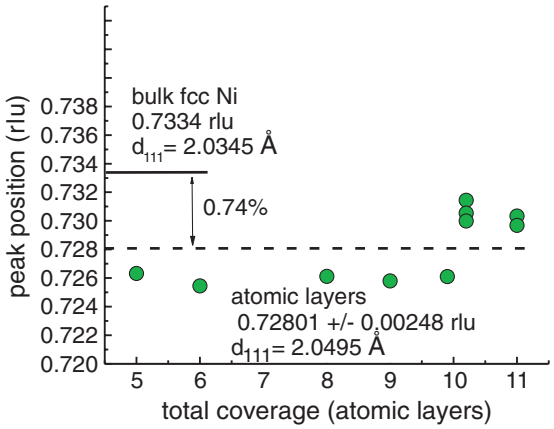

Figure 12. Bragg peak positions from surface x-ray diffraction experiments of Ni(111) films with and without adlayer coverage with the indicated total film thickness in atomic layers [87]. The systems studied are: 5 Ni, 5 Ni +1 Fe, 8 Ni, 8 Ni + 1 Fe, 8 Ni + 1 Fe + 1 Ni, and 10 Ni, 10 Ni + 1 Fe. The data points indicate that a possible adlayer-induced layer relaxation is clearly smaller than 0.001 rlu; see the text. The average layer spacing of the different Ni–adlayer stacks, dashed line, is 0.74% larger as compared to bulk Ni(111).

layers with an *in situ* structural analysis [87]. The deposition of Ni on W(110) leads to the formation of Ni(111) layers, as described by Nishiyama–Wassermann epitaxial growth [75, 124]. The Ni(111) layers show an easy in-plane magnetization direction. Figure 11 indicates that one capping layer of Fe switches the easy magnetization direction of 10 atomic layers Ni from in-plane to out-of-plane, and subsequent deposition of Ni reverts the easy magnetization back to in-plane.

A structural analysis has been performed for Ni(111) films, with and without adlayer coverage. One important result of our detailed structure study [87] is presented in figure 12, which gives the layer spacing for different Ni, and Ni–adlayer systems. We conclude that for a given Ni layer thickness of 5, 8, and 10 atomic layers, the corresponding adlayer-induced structural relaxation is smaller than 0.001 reciprocal lattice units (rlu). This corresponds to an upper limit for the adlayer-induced layer relaxation of 0.003 Å ($\Delta d/d \leqslant 0.0015$).

Can such a small structural change induce an SRT? The magnitude of the corresponding magnetoelastic contribution to the magnetic anisotropy is given by $f_{\rm me} = \frac{1}{6}(B_1(\epsilon_1 - \epsilon_2) + B_2(5\epsilon_1 + \epsilon_2 - 6\epsilon_3))$. With the Ni bulk values $B_1 = 9.38$ MJ m^{-3}, $B_2 = 10$ MJ m^{-3}, and the experimental values for the strain as derived from the structural analysis, $\epsilon_1 = -0.004$, $\epsilon_2 = +0.014, \epsilon_3 = +0.007$, we derive $f_{\rm me} = -0.108$ MJ m^{-3} ($-7.4\,\mu$eV/atom). The negative sign indicates an easy in-plane magnetization direction, in contrast to the experimental result. Magnetoelasticity with Ni bulk values cannot explain the SRT in terms of a subtle structural change. Note, however, that the magnitude and sign of the magnetoelastic coupling coefficients are strain dependent [26], and the discussion of the strain-driven anisotropy must be viewed with caution, as long as no experimental data for the $B_i(\epsilon)$ are available.

However, lattice strain is only one aspect which contributes to the magnetic anisotropy. The adsorption of an atom, or of an adlayer, changes the crystal field near the interface. Consequently, and as discussed in section 2.1 above, adsorbate-induced changes of the crystal field and band filling need to be considered to elucidate the electronic origin of the magnetic anisotropy. The Ni–Fe interlayer hybridization of 3d-orbitals is expected to play a crucial role for this SRT [125].

6. Nano-patterning of magnetic anisotropy

The magnetic anisotropy of ferromagnetic layers can be tuned by a proper selection of the film–substrate combination and by adjusting the growth parameters according to the magnetic requirements. The link between growth parameters and magnetism is given by the correlation between film morphology, film structure and magnetic properties. This correlation is given by the magnetoelastic coupling, and by the length scale of structural and morphological variations as compared to the length scale which describes magnetic properties. Such a magnetic length scale is, for example, the domain wall width $\delta = 4(A/K)^{0.5}$, A: exchange stiffness (Fe: 1×10^{-11} J m^{-1}), K: magnetic anisotropy.

For magnetization reversal by domain motion, an impact of structural and magnetic anisotropy variations on the coercivity is expected, if these variations occur on a length scale which is larger than the domain wall width. Otherwise, the magnetic inhomogeneities are averaged out by the magnetic exchange interactions, and only little impact on the coercivity results [126].

6.1. The self-organized tuning of magnetic anisotropy

The average island size, the island density, the shape of the islands, the formation of misfit dislocation in epitaxially strained systems, and the spacing between misfit dislocations, all depend critically on the details of the growth kinetics, as determined by substrate temperature and film growth rate. Consequently, a change of the film morphology and structure is expected to change the magnetic anisotropy accordingly, and this correlation has been observed in many experiments.

As an example, we discuss the magnetic anisotropy of Fe structures deposited on W(100) [126, 127]. This system shows a rich variety of resulting morphologies from nanoscale Fe islands, to Fe stripes, and flat Fe films, which cover a pseudomorphic Fe capping layer on the W substrate. A key ingredient for the description of the Fe growth is the large misfit of 10% between Fe and W. Therefore, the interplay between strain relaxation and growth kinetics can be exploited to tune the structural and morphological properties.

An example is shown in figure 13, where scanning tunnelling microscopy (STM) images of 4.7 atomic layers of Fe, deposited on W(100), are presented [126, 127]. All images have the same lateral dimensions of 200 nm $\times$ 200 nm, and only the growth temperature has been slightly increased from 360 K in (a) to 440 K in (c). Islands of the fifth layer Fe are shown in grey on top of the four layer thick Fe template, shown in black. Fe islands of the sixth layer are shown in lighter grey. Lines in brighter grey are dislocation lines, which run along $\langle 100 \rangle$ directions, and they are observed only in the five and six layer thick patches.

Due to the coexistence of fully strained Fe with partially relaxed Fe near the dislocation lines, a rather inhomogeneous strain distribution results in the film. The film strain is expected to be relaxed in the direction perpendicular to the dislocation lines, and it is considerably strained along the dislocation lines. This strain variation gives rise to an uniaxial magnetic anisotropy, which is mediated by the magnetoelastic coupling. A spatial variation of the magnetic anisotropy results.

Note that due to the slightly enhanced deposition temperature in (c), the fifth layer Fe island density is considerably reduced. As a consequence, the distance between the dislocation bundles is much smaller in (a) as compared to (c), and also the spacing between the magnetic anisotropy variations, as induced by the strain relaxation, increases from (a) to (c). This has an immediate impact on the coercivity of the Fe film, as shown in (d). The growth condition, which leads to the largest separation between dislocation bundles shown in (c), also induces the

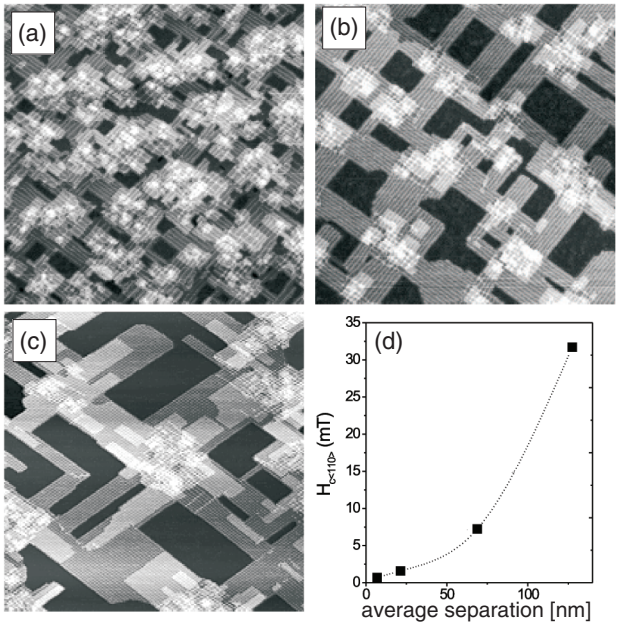

Figure 13. (a)–(c) STM images of 4.7 atomic layers of Fe deposited on W(100) [126]. The image size is 200 nm × 200 nm. The deposition temperature has been slightly increased from 360 K (a) to 440 K (c), which results in a strongly reduced island density of the fifth layer Fe, shown in grey, on the four layer thick Fe template shown in black. See the text for details. (d) A plot of the coercivities for different average separation of the dislocation bundles.

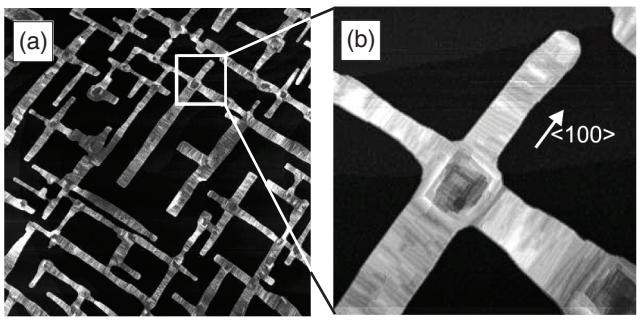

Figure 14. (a)–(b) STM images of 4.7 atomic layers of Fe deposited on W(100) at 500 K [126]. The image size is 1500 nm × 1500 nm in (a), and 300 nm × 300 nm in (b). The legs of the cross are 50 nm wide, the thickness is 1–2 nm.

largest coercivity. Anisotropy variations on a smaller length scale do not induce an appreciable increase of the coercivity; see (d).

Another film morphology is accessible for Fe deposition on W(100) at 500 K; see figure 14 [126]. The same amount of Fe as in figure 13 (4.7 atomic layers) has been deposited; however, at 500 K Ostwald ripening of the Fe structures sets in. The four layer thick Fe template dissolves and acts as a source of additional Fe. Cross-shaped nanostructures with a width of 50 nm and a thickness of 1–2 nm are formed; see figure 14.

These nanoscale Fe crosses have been analysed by scanning electron microscopy with polarization analysis of the secondary electrons (SEMPA), and by micromagnetic simulations.

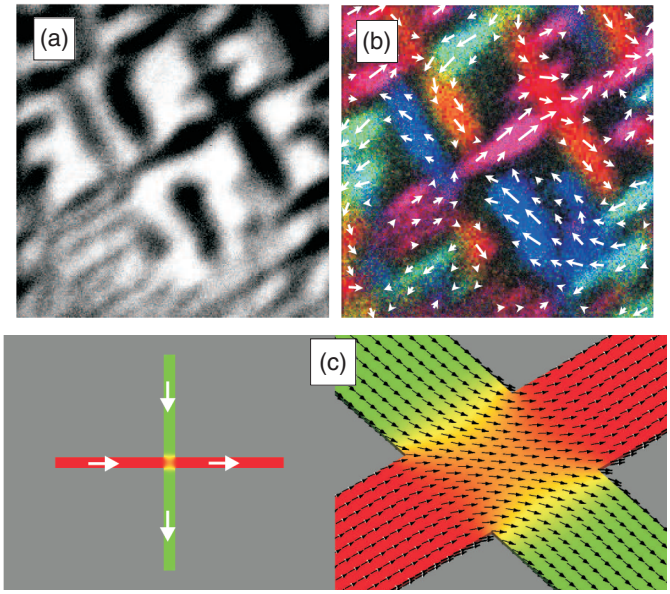

Figure 15. (a) Secondary electron yield image by SEMPA of 4.7 atomic layers of Fe deposited on W(100) at 500 K [126]. Dark areas represent cross-shaped Fe islands. (b) Image of the spin-polarized by SEMPA of the same area. The local magnetization direction is colour-coded and indicated by arrows. (a), (b) Image size: 1500 nm × 1500 nm. (c) Micromagnetic simulation of 50 nm wide cross arms with a thickness of 1.5 nm. The colours and arrows indicate the magnetization direction. This magnetization pattern corresponds to the lowest energy state.

The analysis shows how the magnetization follows the cross morphology, especially at the intersection of cross branches.

The SEMPA investigation shown in figure 15(b) reveals that the magnetization follows the long axis of the branches, which are oriented along the easy magnetization direction of bulk Fe. SEMPA reveals an inhomogeneous magnetization state of the crosses. The magnetization directions of the branches are perpendicular to each other, and the magnetization rotates in-plane at the intersection, so as to establish a smooth transition of the magnetization direction. The micromagnetic simulation of (c) offers an idealized nanoscale magnetization pattern at the intersection, which agrees with the SEMPA analysis.

6.2. The magnetic length scale for nanoscale geometrical constrictions

The domain wall width $\delta = 4(A/K)^{0.5}$ gave the proper magnetic length scale for estimating the critical size, above which structural modulations influence the coercivity of the self-organized Fe nanopattern, as discussed above. The domain wall width is given by the material parameters exchange stiffness A and magnetic anisotropy K. However, in the case of geometrically constrained magnetic structures, like ferromagnetic wires of cross-section S, where the cross-section is reduced to S_0 over a length d, which is smaller than the above calculated Bloch domain wall width, the domain wall properties of the constrained structure are largely determined by the length over which the cross-section changes [128]. Bruno calculated that the domain wall width for a geometrically constrained wall is proportional to the length d of the constriction, and if the constriction has atomic dimensions, the domain wall can be correspondingly narrow, irrespective of the magnetic anisotropy K [128].

Spin-polarized scanning tunnelling spectroscopy has confirmed that the domain wall width is smaller at structural constrictions [129].

7. Magnetic anisotropy on the atomic scale

Recent experimental progress has enabled the study of magnetic properties of single atoms, atomic chains, and nanosize islands. A key element for the preparation of these structures is the controlled deposition of minute amounts of ferromagnetic materials in the (sub)-per cent coverage range, and STM has been applied to image individual atoms or larger structures. The magnetic characterization has been performed by x-ray magnetic dichroism (XMCD) experiments at a synchrotron [42, 43], and by magnetooptical Kerr-effect measurements [130].

These experiments show that the magnetic anisotropy of atoms in reduced dimensionality like chains [42] or in small ensembles with $\approx$10 atoms is considerably enhanced. For an individual Co atom deposited on Pt(111) a large magnetic anisotropy of 9 meV/atom was found from fits to the paramagnetic magnetization curves [43]. The magnetic anisotropy favours an out-of-plane magnetization. Deposition of Co on Pt induces a magnetization of the Pt substrate, and a sizeable contribution to the magnetic anisotropy is expected from the large spin–orbit coupling of Pt [131]. The large magnitude of the anisotropy of 9 meV/atom becomes obvious in comparison to the magnetic anisotropy of the CoPt alloy of 0.8 meV/atom [43]. The magnitude of the magnetic anisotropy per atom decreases rapidly with increasing size of the ensemble, as indicated by the experimental data presented in figure 16.

Figure 16 summarizes some results of an XMCD study, which was performed on Co islands with an average number of atoms $1 \leqslant n_{\mathrm{avg}} \leqslant 40$ [43]. Figures 16(a) and (b) show magnetization curves as obtained from the measured peak intensity at the L_3 absorption edge as a function of the magnetizing field $\mu_0 H$ for an average ensemble size of four (a) and eight atoms (b). The magnetizing field was applied in the out-of-plane direction $\theta = 0°$, or at an angle of 70° with respect to the surface normal. The s-shape of the magnetization curve can be quantitatively ascribed to the paramagnetic response of the Co islands. Note that for both island sizes the out-of-plane magnetization leads to a stronger increase of the Co magnetization (filled circles) as compared to the magnetization along 70° (open squares). This indicates an easy out-of-plane magnetization direction. The magnetic anisotropy energy K is extracted from fits of the magnetization curve. The result for different Co island sizes on Pt(111) is shown in figure 16 (c). The magnetic anisotropy decreases rapidly with increasing island size. This pronounced dependence of K on the island size is already visible in figures 16(a) and (b). The larger slope of the magnetization curve measured at 70° around zero magnetizing field of the average island size of eight atoms (b) as compared to the curve representing an island size of four atoms (a) indicates a reduced magnetic anisotropy in the larger island.

Ab initio calculations of the electronic structure of Co adatoms on the Pt substrate indicate that, in addition to the Co island size, the atomic coordination of the Co adatoms also has a strong influence on the magnetic anisotropy [43]. The calculations suggest a larger magnetic anisotropy for a smaller coordination at the same island size. According to the calculations, the Co-induced polarization of the Pt substrate is another significant source of magnetic anisotropy, which is responsible for 60% of the magnetic anisotropy of the Co pentamer [43].

8. Conclusion and outlook

We have presented examples which elucidate special aspects of the magnetic anisotropy of ultrathin films, as compared to the respective bulk properties. It has been demonstrated

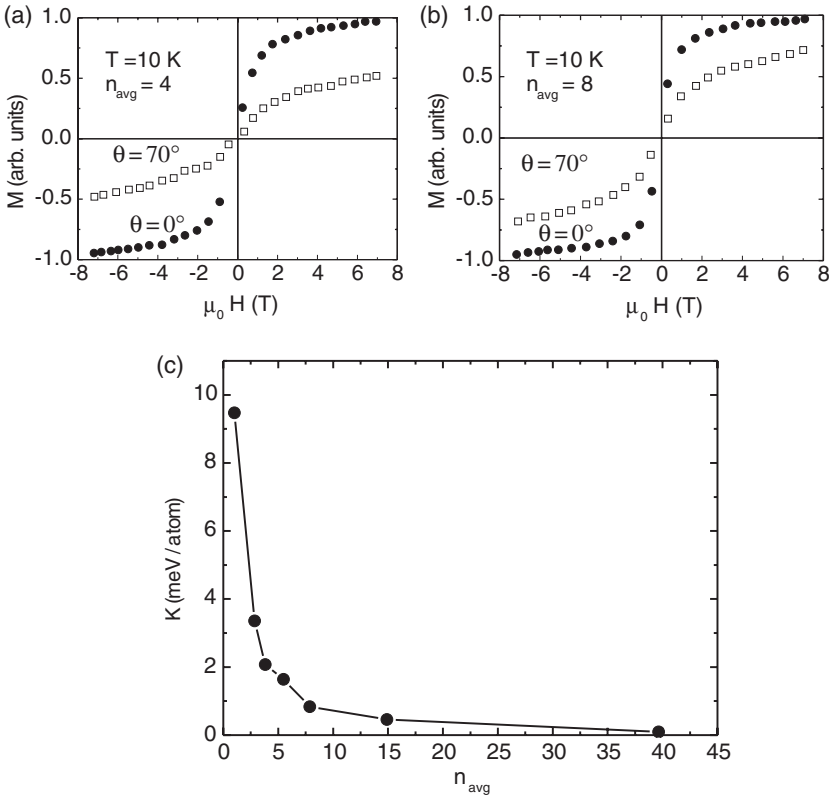

Figure 16. Magnetization of Co islands with an average size of four (a) and eight (b) atoms deposited on Pt(111), as deduced from x-ray absorption measurements. The s-shape magnetization curves can be fitted to a paramagnetic response function, and the fits (not shown) give the magnetic anisotropy, as shown in (c). Note the large magnitude of K for small islands and the pronounced dependence of K on the island size. Experimental data from [43].

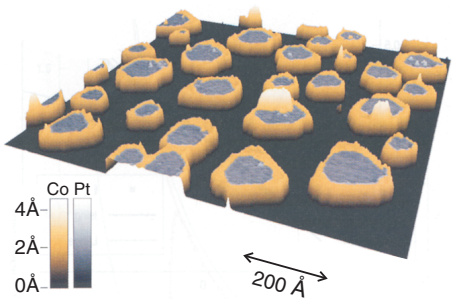

Figure 17. STM image of Pt islands (grey), deposited on Pt(111) (black), where the island perimeter is surrounded by a three-atom-wide Co rim (light grey (orange)). The colour coding exploits the larger apparent height of Co as compared to Pt. Experimental data from [130].

that the relevant magnetic anisotropy contributions are accessible for direct experimental measurements. The application of simplified models, like the 1-over-thickness dependence for the strain relaxation in thin films, is in general not justified. A detailed knowledge of the strain

state of the sample is essential for the proper description of the magnetic anisotropy. However, in addition to strain, an adsorbate coverage has the potential to induce an SRT. Simultaneous strain measurements by surface x-ray diffraction indicate a small magnitude (<0.001) of the adsorbate-induced relative change of the lattice structure. Here, the hybridization between adsorbate and film is essential for the SRT.

The experimental expertise regarding the tuning of island morphology and island size has been applied recently to study the magnetic properties of Co atoms, surrounding Pt islands, prepared on a Pt(111) surface [130]. Figure 17 shows an STM-image of a three-atom-wide layer of Co atoms (light grey (orange)), which surround the perimeter of Pt islands (grey). An analysis of the magnetic susceptibility of the system of figure 17 as compared to compact Co islands of the same size suggests that the perimeter Co atoms determine the magnetic anisotropy decisively. Compact Co islands and the Co–Pt bimetallic islands are found to have the same magnetic anisotropy. This opens a new approach to fine-tune both magnetic anisotropy and total magnetic moment by adjusting the perimeter-to-surface ratio of magnetic nanostructures accordingly [130].

Acknowledgments

The author gratefully acknowledges the continuous support of J Kirschner. I thank W Wulfhekel for the critical reading of the manuscript.

References

[1] Grünberg P 2001 Layered magnetic structures: history highlights applications *Phys. Today* **54** 31–7
[2] Parkin S S P 1998 The magic of magnetic multilayers *IBM J. Res. Dev.* **42** 3–6
[3] Parkin S S P *et al* 1999 Exchange-biased magnetic tunnel junctions and applications to nonvolatile magnetic random access memory *J. Appl. Phys.* **85** 5828–33
[4] Ney A, Pampuch G, Koch R and Ploog K H 2003 Programmable computing with a single magnetoresistive element *Nature* **425** 485–7
[5] Skomski R and Coey J M D 1999 *Permanent Magnetism* (Bristol: Institute of Physics Publishing)
[6] Bruno P 1993 *Magnetismus von Festkörpern und Grenzflächen Physical Origins and Theoretical Models of Magnetic Anisotropy* (Jülich: Forschungszentrum Jülich) pp 24.1–28
[7] Bozorth R M 1993 *Ferromagnetism* (Piscataway, NJ: IEEE)
[8] Kneller E 1962 *Ferromagnetismus* (Berlin: Springer)
[9] Chikazumi S and Charap St H 1964 *Physics of Magnetism* (Malabar, FL: Krieger)
[10] Carr W J Jr 1966 *Secondary Effects in Ferromagnetism* (*Handbuch der Physik* vol Band XVIII/2) (Berlin: Springer)
[11] Blundell St 2001 *Magnetism in Condensed Matter* (Oxford: Oxford University Press)
[12] Gradmann U 1988 *Surfaces Interfaces and Ultrathin Films* (*Landolt–Börnstein Numerical Data and Functional Relationships in Science and Technology* Group III, vol 19) (Berlin: Springer)
[13] Gradmann U 1993 *Magnetism in Ultrathin Transition Metal Films* (*Handbook of Magnetic Materials* vol 7) (Amsterdam: Elsevier Science) chapter 1, pp 1–96
[14] Gradmann U 1994 *Magnetic Properties of Single Crystal Surfaces* (*Landolt–Börnstein Numerical Data and Functional Relationships in Science and Technology* Group III, vol 24) (Berlin: Springer)
[15] Bland J A C and Heinrich B (ed) 1994 *Ultrathin Magnetic Structures* vol I (Berlin: Springer)
[16] Bland J A C and Heinrich B (ed) 1994 *Ultrathin Magnetic Structures* vol II (Berlin: Springer)
[17] Baberschke K, Donath M and Nolting W (ed) 2001 *Band-Feromagnetism* (*Lecture Notes in Physics; Physics and Astronomy*) (Berlin: Springer)
[18] Bruno P and Renard J-P 1989 Magnetic surface anisotropy of transition metal ultrathin films *Appl. Phys.* A **49** 1833–5
[19] Heinrich B, Cochran J F, Arott A S, Purcell S T, Urqhart K B, Dutcher J R and Egelhoff W F Jr 2003 Stress and growth of Ag monolayers on a Fe(100) whisker *Phys. Rev.* B **68** 045416
[20] Siegmann H C 1992 Surface and 2D magnetism *J. Phys.: Condens. Matter* **4** 8395–434
[21] Prinz G A 1992 Magnetic anisotropy in epitaxial metal films *Ultramicroscopy* **47** 346–54

[22] de Jonge W J M, Bloemen P J H and den Broeder F J A 1994 *Experimental Investigation of Magnetic Anisotropy* (*Ultrathin Magnetic Structures* vol I) (Berlin: Springer)
[23] Elmers H J, Hauschild J, Fritzsche H, Liu G, Gradmann U and Köhler U 1995 Stress evolution during the growth of ultrathin layers of iron and iron silicide on Si(111) *Phys. Rev. Lett.* **75** 2031–4
[24] Johnson M T, Bloemen P J H, den Broeder F J A and de Vries J J 1996 Magnetic anisotropy in metallic multilayers *Rep. Prog. Phys.* **59** 1409–58
[25] Farle M 1998 Ferromagnetic resonance of ultrathin metallic layers *Rep. Prog. Phys.* **61** 755–826
[26] Sander D 1999 The correlation between mechanical stress and magnetic anisotropy in ultrathin films *Rep. Prog. Phys.* **62** 809–58
[27] Sander D, Ouazi S, Enders A, Gutjahr-Löser Th, Stepanyuk V S, Bazhanov D I and Kirschner J 2002 Stress strain and magnetostriction in epitaxial films *J. Phys.: Condens. Matter* **14** 4165–76
[28] Himpsel J F, Ortega J E, Mankey G J and Willis R F 1998 Magnetic nanostructures *Adv. Phys.* **47** 511–97
[29] Skomski R 2003 Nanomagnetics *J. Phys.: Condens. Matter* **15** R841–96
[30] Sellmyer D J, Zheng M and Skomski R 2001 Magnetism of Fe, Co, and Ni nanowires in self-assembled arrays *J. Phys.: Condens. Matter* **13** R433–60
[31] Mills D L 1994 *Thermodynamic Properties of Ultrathin Films* (*Ultrathin Magnetic Structures* vol I) (Berlin: Springer) chapter 3, pp 92–121
[32] van Vleck J H 1945 A survey of the theory of ferromagnetism *Rev. Mod. Phys.* **17** 27–47
[33] Kittel C 1963 *Introduction to Solid State Physics* (New York: Wiley)
[34] Brooks H 1940 Ferromagnetic anisotropy and the itinerant electron model *Phys. Rev.* **58** 909–18
[35] Trygg J, Johansson B, Eriksson O and Wills J M 1995 Total energy calculation of magnetocrystalline anisotropy energy in the ferromagnetic 3d metals *Phys. Rev. Lett.* **75** 2871–4
[36] Burkert T, Eriksson O, James P, Simak S I, Johansson B and Nordström L 2004 Calculation of uniaxial magnetic anisotropy energy of tetragonal and trigonal Fe, Co, Ni *Phys. Rev.* B **69** 104426
[37] Ravindran P, Kjekshus A, Fjelvåg H, James P, Nordström L, Johansson B and Eriksson O 2001 Large magnetocrystalline anisotropy in bilayer transition metal phases from first-principles full-potential calculations *Phys. Rev.* B **63** 144409
[38] Wu R, Chen L J, Shick A and Freeman A J 1998 First-principles determinations of magneto-crystalline anisotropy and magnetostriction in bulk and thin-film transition metals *J. Magn. Magn. Mater.* **177–181** 1216–9
[39] Daalderop G H, Kelly P J and den Broeder F J A 1992 Prediction and confirmation of perpendicular magnetic anisotropy in Co/Ni multilayers *Phys. Rev. Lett.* **68** 682–5
[40] Újfalussy B, Szunyogh L, Bruno P and Weinberger P 1996 First-principles calculation of the anomalous perpendicular anisotropy in a Co monolayer on Au(111) *Phys. Rev. Lett.* **77** 1805–8
[41] Kuch W 2003 X-ray magnetic circular dichroism for quantitative element-resolved magnetic microscopy *Phys. Scr.* at press
[42] Gambardella P, Dhesi S S, Gardonio G, Grazioli C, Ohresser P and Carbone C 2002 Localized magnetic states of Fe, Co, and Ni impurities on alkali metal films *Phys. Rev. Lett.* **88** 047202
[43] Gambardella P, Rusponi S, Veronesa M, Dhesi S S, Grazioli C, Dallmeyer A, Cabria I, Zeller R, Dederichs P H, Kern K, Carbone C and Brune H 2003 Giant magnetic anisotropy of single cobalt atoms and nanoparticles *Science* **300** 1130–3
[44] Elmers H J and Gradmann U 1990 Magnetic anisotropies in Fe(110) films on W(110) *Appl. Phys.* A **51** 255–63
[45] Weber W, Bischof A, Allenspach R, Back C H, Fassbender J, May U, Schirmer B, Jungblut R M, Güntherodt G and Hillebrands B 1996 Structural relaxation and magnetic anisotropy in Co/Cu(001) films *Phys. Rev.* B **54** 4075–9
[46] Oepen H P, Millev Y T, Ding H F, Pütter S and Kirschner J 2000 Field-driven reorientation in ultrathin ferromagnetic films with uniaxial anisotropy *Phys. Rev.* B **61** 9506–12
[47] Wulfhekel W, Gutjahr-Löser Th, Zavaliche F, Sander D and Kirschner J 2001 Relation between structure stress and magnetism in Co/W(001) *Phys. Rev.* B **64** 144422
[48] Stearns M B 1986 *Magnetic Properties of 3d, 4d and 5d Elements Alloys and Compounds* (*Landolt–Börnstein Numerical Data and Functional Relationships in Science and Technology* Group III, vol 19a) (Berlin: Springer)
[49] Farle M, Plotow W, Anisimov A N, Poulopoulos P and Baberschke K 1997 Anomalous reorientation phase transition of the magnetization in fct Ni/Cu(001) *Phys. Rev.* B **56** 5100
[50] Wu R 2001 First principles determination of magnetic anisotropy and magnetostriction in transition metal alloys *(Lecture Notes in Physics: Band-Ferromagnetism)* (Berlin: Springer) part I, pp 46–71
[51] Eriksson O 2001 First principles theory of magnetism for materials with reduced dimensionality *(Lecture Notes in Physics: Band-Ferromagnetism)* (Berlin: Springer) part IV, pp 243–66

[52] Heinrich B and Cochran J F 1993 Ultrathin metallic magnetic films: magnetic anisotropies and exchange interaction *Adv. Phys.* **42** 523–639
[53] Chuang D S, Ballentine C A and O'Handley R C 1994 Surface and step magnetic anisotropy *Phys. Rev.* B **49** 15084–95
[54] Shick A B, Gornostyrev Y N and Freeman A J 1999 Magnetoelastic mechanism of spin-reorientation transition at step edges *Phys. Rev.* B **60** 3029–32
[55] Mireles H C and Erskine J L 2001 Surface-step induced double magnetic switching of Fe on vicinal W(001) *Phys. Rev. Lett.* **87** 037201
[56] Bruno P 1988 Magnetic surface anisotropy of cobalt and surface roughness effects within Néel's model *J. Phys. F: Met. Phys.* **18** 1291–8
[57] Kittel C 1949 Physical theory of ferromagnetic domains *Rev. Mod. Phys.* **21** 541–83
[58] Schulz B and Baberschke K 1994 Crossover from in-plane to perpendicular magnetization in ultrathin Ni/Cu(001) films *Phys. Rev.* B **50** 13467–71
[59] Vollmer R, Gutjahr-Löser Th, Kirschner J, van Dijken S and Poelsema B 1999 Spin reorientation transition in Ni films on Cu(001): the influence of H_2 adsorption *Phys. Rev.* B **60** 6277–80
[60] Wedler G, Walz J, Greuer A and Koch R 1999 Stress dependence of the magnetoelastic coupling constants B1 and B2 of epitaxial Fe(001) *Phys. Rev.* B **60** R11313–6
[61] Sander D, Ouazi S, Enders A, Gutjahr-Löser Th, Stepanyuk V S, Bazhanov D I and Kirschner J 2002 Stress strain and magnetostriction in epitaxial films *J. Phys.: Condens. Matter* **14** 4165–76
[62] Sander D, Meyerheim H, Ferrer S and Kirschner J 2003 Stress strain and magnetic anisotropy: all is different in nanometer thin films *Adv. Solid State Phys.* **43** 547–61
[63] Sander D 2003 Surface stress: implications and measurements *Curr. Opin. Solid State Mater. Sci.* **1** 51–7
[64] Ibach H 1997 The role of surface stress in reconstruction epitaxial growth and stabilization of mesoscopic structures *Surf. Sci. Rep.* **29** 193–264
[65] Dahmen K, Ibach H and Sander D 2001 A finite element analysis of the bending of crystalline plates due to anisotropic surface and film stress applied to magnetoelasticity *J. Magn. Magn. Mater.* **231** 74–84
[66] Dahmen K, Lehwald S and Ibach H 2000 Bending of crystalline plates under the influence of surface stress *Surf. Sci.* **446** 161–73
[67] Hjortstam O, Baberschke K, Wills J M, Johansson B and Eriksson O 1997 Magnetic anisotropy and magnetostriction in tetragonal and cubic Ni *Phys. Rev.* B **55** 15026–32
[68] Fähnle M and Komelj M 2000 Nonlinear magnetoelastic coupling coefficients from simultaneous measurements of magnetostrictive stress and anisotropy in epitaxial films *J. Magn. Magn. Mater.* **220** L13–7
[69] Fähnle M, Komelj M, Wu R Q and Guo G Y 2002 Magnetoelasticity of Fe: possible failure of *ab initio* electron theory with the local-spin-density approximation and with the generalized-gradient approximation *Phys. Rev.* B **65** 144436
[70] Komelj M and Fähnle M 2002 Shear-strain related nonlinear magnetoelastic properties of epitaxial films *Phys. Rev.* B **65** 092403
[71] Komelj M and Fähnle M 2002 On the magnetoelastic contribution to the magnetic anisotropy of thin epitaxial Permalloy films: an *ab initio* study *J. Magn. Magn. Mater.* **238** L125–8
[72] Wu R and Freeman A J 1996 First principles determination of magnetostriction in transition metals *J. Appl. Phys.* **79** 6209–12
[73] Zangwill A 1988 *Physics at Surfaces* (Cambridge: Cambridge University Press)
[74] Mahesh R, Sander D, Zharkov S M and Kirschner J 2003 Stress and growth of Ag monolayers on a Fe (100) whisker *Phys. Rev.* B **68** 045416
[75] Meyerheim H L, Sander D, Popescu R, Kirschner J, Robach O, Ferrer S and Steadman P 2003 Ni-induced giant stress and surface relaxation in W(110) *Phys. Rev.* B **67** 155422
[76] Heinz K, Müller S and Hammer L 1999 Crystallography of ultrathin iron cobalt and nickel films grown epitaxially on coper *J. Phys.: Condens. Matter* **11** 9437–54
[77] Hearmon R F S 1969 *The Elastic Constants of Non-Piezoelectric Crystals* (*Landolt–Börnstein Numerical Data and Functional Relationships in Science and Technology* Group III, vol 2) (Berlin: Springer)
[78] Hearmon R F S 1984 *The Elastic Constants of Crystals and Other Anisotropic Materials* (*Landolt–Börnstein Numerical Data and Functional Relationships in Science and Technology* Group III, vol 18) (Berlin: Springer)
[79] Matthews J W and Crawford J L 1970 Accommodation of misfit between single-crystal films of nickel and copper *Thin Solid Films* **5** 187–98
[80] Matthews J W and Blakeslee A E 1974 Defects in epitaxial multilayers, i. Misfit dislocations *J. Cryst. Growth* **27** 118–25
[81] Matthews J W and Blakeslee A E 1975 Defects in epitaxial multilayers, ii. Dislocation pile-ups threading dislocations, slip lines and cracks *J. Cryst. Growth* **29** 273–80

[82] Nix W D 1989 Mechanical properties of thin films *Metall. Trans.* A **20A** 2217–45
[83] Chappert C and Bruno P 1988 Magnetic anisotropy in metallic ultrathin films and related experiments on cobalt *J. Appl. Phys.* **64** 5736–41
[84] Enders A 1999 Mechanische Spannungen und Ferromagnetismus ultradünner Schichten *PhD Thesis* Martin-Luther Universität Halle-Wittenberg, Mathematisch-Naturwissenschaftlich-Technische Fakultät
[85] Gutjahr-Löser Th 1999 Magnetoelastische Kopplung in oligatomaren Filmen *PhD Thesis* Martin-Luther Universität Halle-Wittenberg, Mathematisch-Naturwissenschaftlich-Technische Fakultät
[86] Popescu R, Meyerheim H L, Sander D, Kirschner J, Steadman P, Robach O and Ferrer S 2003 Surface x-ray structure analysis of periodic misfit dislocations in Fe/W(110) *Phys. Rev.* B **68** 155421-1–11
[87] Meyerheim H L, Sander D, Popescu R, Kirschner J, Robach O and Ferrer S 2004 Upper limit of structural relaxation upon adlayer-induced spin reorientation transition of nickel monolayers *Phys. Rev.* B submitted
[88] Gutjahr-Löser Th, Sander D and Kirschner J 2000 Magnetoelastic coupling in Ni and Fe monolayers on Cu(001) *J. Appl. Phys.* **87** 5920–2
[89] Sander D, Enders A and Kirschner J 1999 Stress and magnetic properties of surfaces and ultrathin films *J. Magn. Magn. Mater.* **200** 439–55
[90] Gutjahr-Löser Th, Sander D and Kirschner J 2000 Magnetoelastic coupling in Co thin films on W(001) *J. Magn. Magn. Mater.* **220** L1–7
[91] Markov I V 1995 *Crystal Growth for Beginners: Fundamentals of Nucleation Crystal Growth and Epitaxy* (Singapore: World Scientific)
[92] King D A (ed) 1997 *Growth and Properties of Ultrathin Epitaxial Layers* (*The Chemical Physics of Solid Surfaces* vol 8) (Amsterdam: Elsevier)
[93] Koch R 1997 *Intrinsic Stress of Epitaxial Thin Films and Surface Layers* (*The Chemical Physics of Solid Surfaces* vol 8) (Amsterdam: Elsevier)
[94] Bruno P 1988 Dipolar magnetic surface anisotropy in ferromagnetic thin films with interfacial roughness *J. Appl. Phys.* **64** 3153–6
[95] Poulopoulos P, Lindner J, Farle M and Baberschke K 1999 Change of magnetic anisotropy due to roughness: a quantitative scanning tunneling microscopy study on Ni/Cu(001) *Surf. Sci.* **437** 277–84
[96] Reuter D, Gerth G and Kirschner J 1997 Surface diffusion of 3d-metals on W(110) *Surface Diffusion: Atomistic and Collective Processes* (New York: Plenum)
[97] Reuter D, Gerth G and Kirschner J 1998 Anisotropic diffusion of 3d metals on W(110): competition between crystalline structure and surface steps *Phys. Rev.* B **57** 2520–9
[98] Sander D, Skomski R, Enders A, Schmidthals C, Reuter D and Kirschner J 1998 The correlation between mechanical stress and magnetic properties of ultrathin films *J. Phys. D: Appl. Phys.* **31** 663–70
[99] Lu L, Bansmann J and Meiwes-Broer K H 1998 Rotation of the easy-magnetization direction upon the phase transition from thin iron films to islands on W(110) *J. Phys.: Condens. Matter* **10** 2873–80
[100] Aharoni A 1998 Demagnetizing factors for rectangular ferromagnetic prisms *J. Appl. Phys.* **83** 3432–4
[101] Stepanyuk V S, Tsivlin D V, Sander D, Hergert W and Kirschner J 2003 Mesoscopic scenario of strain-relief at metal interfaces *Thin Solid Films* **43** 1–5
[102] Pan W, Sander D, Lin M T and Kirschner J 2003 Stress oscillations and surface alloy formation during the growth of FeMn on Cu(001) *Phys. Rev.* B **68** 224419-1–5
[103] Osborn J A 1945 Demagnetizing factors of the general ellipsoid *Phys. Rev.* **67** 351–7
[104] Draaisma H J G and de Jonge W J M 1988 Surface and volume anisotropy from dipole–dipole interactions in ultrathin films *J. Appl. Phys.* **64** 3610–3
[105] Vedmedenko E Y, Oepen H P and Kirschner J 2003 Size-dependent spin reorientation transition in nanoplatelets *Phys. Rev.* B **67** 012409
[106] Vedmedenko E Y, Oepen H P and Kirschner J 2003 Size-dependent magnetic properties of nanoplatelets *J. Magn. Magn. Mater.* **256** 237–42
[107] Millev Y T, Vedmedenko E Y and Oepen H P 2003 Dipolar magnetic anisotropy energy of laterally confined ultrathin ferromagnets *J. Phys. D: Appl. Phys.* **36** 2945–9
[108] Heinrich B 1994 *Ferromagnetic Resonance in Ultrathin Film Structures* (*Ultrathin Magnetic Structures* vol II) (Berlin: Springer) chapter 3.1, pp 195–222
[109] Cochran J F 1994 *Light Scattering from Ultrathin Magnetic Layers and Bilayers* (*Ultrathin Magnetic Structures* vol II) (Berlin: Springer) chapter 3.2, pp 222–57
[110] Hillebrands B and Güntherodt G 1994 *Brillouin Light Scattering in Magnetic Superlattices* (*Ultrathin Magnetic Structures* vol II) (Berlin: Springer) chapter 3.3, pp 258–96
[111] Gradmann U and Müller J 1968 *Phys. Status Solidi* **27** 313–24
[112] Bader S D and Erskine J L 1994 *Magneto-Optical Effects in Ultrathin Films* (*Ultrathin Magnetic Structures* vol II) (Berlin: Springer) chapter 4, pp 297–325

[113] Kuch W 2003 Edge atoms do all the work *Nat. Mater.* **2** 505–6
[114] Gambardella P, Dallmeyer A, Maiti K, Malagoli M C, Eberhardt W, Kern K and Carbone C 2002 Ferromagnetism in one-dimensional monoatomic metal chains *Nature* **416** 301–4
[115] Arnold C S and Pappas D P 2000 Gd(001): a semi.infinite three-dimensional Heisenberg ferromagnet with ordinary surface transition *Phys. Rev. Lett.* **85** 5202–5
[116] Arnold C S, Pappas D P and Popov A P 1999 Second- and first-order phase transitions in the magnetic reorientation of ultrathin Fe on Gd *Phys. Rev. Lett.* **83** 3305–8
[117] Baberschke K 2001 Anisotropy in magnetism *(Lecture Notes in Physics: Band-Ferromagnetism)* (Berlin: Springer) part I, pp 27–45
[118] Poulopoulos P and Baberschke K 1999 Magnetism in thin films *J. Phys.: Condens. Matter* **11** 9495–515
[119] Li Y and Baberschke K 1992 Dimensional crossover in ultrathin Ni(111) films on W(110) *Phys. Rev. Lett.* **68** 1208–11
[120] Farle M, Mirwald-Schulz B, Anisimov A N, Plotow W and Baberschke K 1997 Higher-order magnetic anisotropies and the nature of the spin-reorientation transition in face-centered-tetragonal Ni(001)/Cu(001) *Phys. Rev.* B **55** 3708–15
[121] Maca F, Shick A B, Podloucky R and Weinberger P 2003 The influence of hydrogen adsorption on magnetic properties of Ni/Cu(001) surface *Czech. J. Phys.* **53** 33–9
[122] Sander D, Enders A, Schmidthals C, Kirschner J, Johnston H L and Venus D 1997 Structure and perpendicular magnetization of Fe/Ni(111) bilayers on W(110) *J. Appl. Phys.* **81** 4702–5
[123] Matsumura D, Yokoyama T, Amemiya K, Kitagawa S and Ohta T 2002 X-ray magnetic circular dichroism study of spin reorientation transition of magnetic thin films induced by surface chemisorption *Phys. Rev.* B **66** 024402
[124] Sander D, Schmidthals C, Enders A and Kirschner J 1998 Stress and structure of Ni monolayers on W(110): the importance of lattice mismatch *Phys. Rev.* B **57** 1406–9
[125] Skomski R, Sander D, Schmidthals C, Enders A and Kirschner J 1998 Iron and nickel surface and interface anisotropies *IEEE Trans. Magn.* **34** 852–4
[126] Wulfhekel W, Zavaliche F, Hertel R, Bodea S, Steierl G, Liu G, Oepen H P and Kirschner J 2003 Growth structure and magnetism of Fe nanostructures on W(001) *Phys. Rev.* B **68** 144416
[127] Wulfhekel W, Zavaliche F, Poratti F, Oepen H P and Kirschner J 2000 Nano-patterning of magnetic anisotropy by controlled strain relief *Europhys. Lett.* **49** 651–7
[128] Bruno P 1999 Geometrically constrained magnetic wall *Phys. Rev. Lett.* **83** 2425–8
[129] Pietzsch O, Kubetzka A, Bode M and Wiesendanger R 2000 Real-space observation of dipolar antiferromagnetism in magnetic nanowires by spin-polarized scanning tunneling spectroscopy *Phys. Rev. Lett.* **84** 5212–5
[130] Rusponi S, Cren T, Weiss N, Epple M, Buluschek P, Claude L and Brune H 2003 The remarkable difference between surface and step atoms in the magnetic anisotropy of two-dimensional nanostructures *Nat. Mater.* **2** 546–51
[131] James P, Eriksson O, Hjortstam O, Johansson B and Nordström L 2000 Calculated trends of the magnetostriction coefficient of 3d alloys from first principles *Appl. Phys. Lett.* **76** 915–7